Composite Structures 163 (2017) 168–184

Contents lists available at ScienceDirect

Composite Structures

journal homepage: www.elsevier.com/locate/compstruct

A hierarchical finite element for composite laminated beams using a refined zigzag theory

Liz G. Nallim [a,*], Sergio Oller [b], Eugenio Oñate [b], Fernando G. Flores [c]

[a] INIQUI-CONICET. Facultad de Ingeniería, Universidad Nacional de Salta, Av. Bolivia 5150, 4400 Salta, Argentina
[b] UPC–CIMNE. Centro Internacional de Métodos Numéricos en Ingeniería, España. Universidad Politécnica de Cataluña (Barcelona-Tech), Campus Norte UPC, 08034 Barcelona, España
[c] IDIT – Departamento de Estructuras, Universidad Nacional de Córdoba and CONICET, Av. Velez Sarsfield 1611, 5016 Córdoba, Argentina

ARTICLE INFO

Article history:
Received 28 October 2016
Revised 6 December 2016
Accepted 6 December 2016
Available online 10 December 2016

Keywords:
Refined zigzag theory
Hierarchical finite element method
PRZ element
Beam finite element
Composite beam
Laminated beam

ABSTRACT

In this work a kinematics for laminated beams enriched with a refined formulation ZigZag (RZT), originally presented by Tessler et al. in 2007, introduced in a hierarchical one dimensional type "p" finite element is presented. The finite element employs Lagrange polynomials for the approximation of the degrees of freedom of the ends (nodes) and orthogonal Gram-Schmidt polynomials to the internal degrees of freedoms. This finite element allows a very low discretization, is free of shear locking and behaves very well when the analysis of laminated composites with accurate determination of local stresses and strains at laminar level is necessary.

This element has been validated in the analysis of laminated beams with various sequences of symmetric and asymmetric stacking, studying in each case its accuracy and stability.

1. Introduction and review

Laminated composite beams are basic components for several structural engineering applications, due to their excellent mechanical properties, namely high specific strength and stiffness, long fatigue life, wear resistance and enhanced design freedom on a micro- and macro-mechanical level. The behavior of laminated beams is governed by a wide number of parameters due to their complex behavior. Moreover, specific problems arise such as delamination and complex damage and failure mechanisms that need a proper modeling for an accurate appraisal of the study of their mechanics. In particular, as it is shown by Carrera [1–2], a slope discontinuity on the displacement field occurs at the interface between two perfectly bonded layers because of the transverse anisotropy, i.e. the difference in layer-wise transverse shear and normal moduli. This is known as the ZigZag (ZZ) phenomenon.

Considering theses aspects a number of theories have been proposed for the analysis of composite laminates. Theories used for the through –thickness variation of the state variables (unknowns are of displacement type) can be classified as: equivalent single layer models (ESL), layer-wise models (LW) and zigzag models (ZZ). The well-described unified formulation, initially presented by Carrera [3] and extended by Demasi [4–8], describes precisely and clearly the models, types and class of these theories.

In the ESL theories the assumed displacements vary continuously across the laminate thickness and the number of unknowns is independent of the number of layers. ESL models include mainly three major categories, i.e., the classical theory (CT), the first-order theory (FDT), and the higher-order theory (HOT). The CT known as Euler–Bernoulli beam theory is the simplest one and is inaccurate for reasonably thick laminated beams and/or for highly anisotropic composite beams. The inaccuracy is due to neglecting the transverse shear strains in the laminate. The FDT by Timoshenko [9] considers constant transverse shear strain distribution through the beam thickness and, thus, a shear correction factor has to be incorporated to adjust the transverse shear stiffness. The accuracy of FDT solutions depend on the shear correction factor which cannot in general be determined a priori apart from very special cases [10]. Moreover, FDT produces piecewise constant transverse shear stresses that violate the interlaminar continuity (IC) conditions and the traction-free conditions at the top and bottom surfaces. To overcome these shortcomings and to avoid the use of shear correction factors, a number of high-order theories with different shear strain shape functions were introduced. In general, the cross section is allowed to deform in any form by including higher order terms in the axiomatic expansion of the displacement field along

* Corresponding author at: INIQUI-CONICET. Facultad de Ingeniería, Universidad Nacional de Salta, Av. Bolivia 5150, 4400 Salta, Argentina.
E-mail address: lnallim@unsa.edu.ar (L.G. Nallim).

http://dx.doi.org/10.1016/j.compstruct.2016.12.031
0263-8223/

the beam direction (x-axis) as a suitable smooth function of transverse direction (z-axis). In this sense different shape functions have been proposed such as polynomial [11–14], trigonometric [15–18], exponential [19–21] and hyperbolic functions [22,23]. Carrera et al. [24] discussed a number of refined beam theories which were obtained expanding the unknown displacement variables over the beam section axes by adopting Taylor's polynomials, trigonometric series, exponential, hyperbolic and zigzag functions, by using the Unified Formulation introduced by Carrera [3]. A class of theories often included into HOT are the advanced higher order theories, denoted as AHOT, where transverse normal strains are incorporated by extending the expansion of the transverse displacement. For instance, Vidal et al. [25] proposed the approximation of the displacement field as a sum of separated functions of axial and transverse coordinate by adopting the Proper Generalized Decomposition procedure. HOT gives a continuous variation of the transverse shear strain across the thickness but shows discontinuity in the shear stress distribution at the layer interfaces (if they are computed through the constitutive equations) due to different values of shear rigidity at the adjacent layers. But the actual behavior of a composite laminate is opposite i.e., the transverse shear stress must be continuous at the layer interface and the corresponding strain may be discontinuous [26].

In LW models [27–34] the displacement field within each layer is prescribed and compatibility conditions are applied between adjacent layers in the laminate to recover the model of the laminate as a whole. These models provide realistic descriptions of kinematics at the ply level and they have the capacity to take into account the zigzag effect. However, LW approaches suffer from an excessive number of displacement variables in proportion to the number of layers and hence they are too expensive in terms of computational cost and hardly appropriate for practical applications.

ZigZag models include a set of layer independent theories in which a LW discontinuous function is a priori selected to enrich the kinematical model in such way that the interface conditions are met. So, in these theories, the in-plane displacements have piece-wise variation across the beam thickness and the number of unknowns results independent of the number of layer. Examples of ZZ theories are those found in articles published by Murakami [35], Lee et al. [36], Cho and Paramerter [37], Cho and Averill [38], Vidal and Polit [39,40].

The research activity about the modeling of laminated structural members and the corresponding analytical or numerical solutions are numerous. In particular, as this paper is devoted to ZigZag models a complete and extensive assessment about the subject can be found in Carrera [1]. Other reference in the topic is the review paper by Chakrabarti et al. [26]. On the other side, Groh and Weaver [41] present, in the article introduction, a comprehensive overview of the different theories that are used for the analysis of highly heterogeneous laminated beams.

Many ZigZag theories requires C^1 continuity for the deflection field, which is a drawback versus simpler C^0 continuous FEM approximations [42]. Tessler et al. [43–45] developed a refined zigzag theory (RZT) that allows the use of C^0 continuous interpolation for all the kinematic variables. The kinematics of RZT is essentially that of FDT enhanced by a zigzag field which has the property of vanishing on the top and bottom surface of the laminate.

Along with the development of beam theories, there has been significant development towards the solution methodologies. Analytical solutions are applicable for a few particular classes of beam configuration [46,47]. The development of computational technologies makes it quite possible to implement numerical methods for the practical applications. Among these, FEM is most popular and versatile method for investigating the structural behavior of arbitrary shaped components. In this context Oñate et al. [42] developed a simple 2-noded beam element based on the RZT theory, where shear locking is avoided using reduced integration on selected terms of the shear stiffness matrix. The classical version or h version of FEM was used in this paper, where the accuracy of the solution is achieved by refinement of finite element mesh.

Unlike the h FEM version, in the p version of FEM the mesh remains constant while the degree of the interpolation polynomial is gradually increased to the desired accuracy [48]. The degrees of freedom of a p element are constituted by the degrees of freedom of the one-dimensional element ends (nodes) and the amplitudes of the shape functions within the element. The p-version is characterized by being more robust than the version h [49], in other words the performance of the p-version is much less sensitive to input data tan the h-version. For example, the p version allows proper treatment of elements with high slenderness, as it is free of shear locking. This is especially important in the analysis of laminated composite beams, where a more rigorous stress analysis at laminar and inter-laminar level is necessary. Several demonstrative examples and theoretical proofs of the advantages of the p-version FEM can be found in the literature [48,50–54]. Recall that the advantages of the p version are not limited to the greater convergence rate. In fact, with h methods, the accuracy of the solution is determined by executing several analyses with different meshes, an expensive and time-consuming process, both because of the computational cost and because of the operator time required to define the different models. In p-convergent approximations, the number of finite elements is determined by the geometry and is small [55].

In this paper a hierarchical one-dimensional finite element, based on the ZigZag refined theory by Tessler et al. [43–45] is proposed. This finite element has two end nodes and four degrees of freedom per node. To approximate the kinematics variables of this formulation Lagrange polynomials as local support functions are used, and orthogonal polynomials generated by means of recurrence Gram-Schmidt expressions [58–59] are employed as functions of hierarchical enrichment [60–63]. It is necessary to emphasize here that one of the main novelty of the proposed model is the obtaining of a hierarchical finite element within the framework of a Zig-Zag theory, considering local support functions of C_0 type and achieving a robust finite element free of shear locking. Besides, the developed formulation is appropriated for the analysis of symmetric and non-symmetric laminated beams in a general and unified way, since all mechanical coupling are considered. Another important and salient feature of the developed model is the capacity it has for its application to the delamination study as will be seen in Section 8.

The proposed finite element has been computationally implemented. To verify the results, the order of the approximation can be selectively increased. This operation is carried out very efficiently because it is not necessary to generate a new mesh and because the new linear stiffness matrix contains the preceding one. It is demonstrated that the proposed hierarchical finite element is free of shear locking and, in order to assess its accuracy and stability, it has been applied to the analysis of laminated beams with symmetrical and non-symmetrical stacking sequence with different boundary conditions.

2. Formulation of the mechanical problem

Let us consider a laminated beam of total thickness h and length L as shown in Fig. 1. The Cartesian coordinate system (x,y,z) is taken such that the $x-y$ plane $(z=0)$ coincides with the midplane of the beam, the y axis is along the width (b) of the beam; resulting in a beam domain

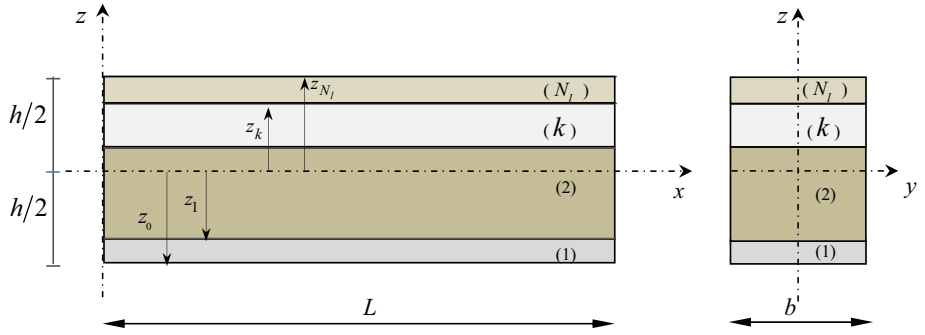

Fig. 1. Multilayered composite beam geometry.

$V = [0 \leqslant x \leqslant L] \times [-b/2 \leqslant y \leqslant b/2] \times [-h/2 \leqslant z \leqslant h/2]$. The displacement vector is $\mathbf{u} = (u, v, w)$ and the displacement components along each coordinate axis are designed by u, v, w. The laminated beam is composed of N_l layers of different linearly elastic materials, being each layer orthotropic in the beam axes. The integer k, used as superscript or subscript, denotes the layer number from the bottom to the top of the beam; thus the kth layer corresponds to $z_{k-1} \leqslant z \leqslant z_k$ and its thickness is h_k.

The one dimensional constitutive equations of the kth layer of an orthotropic material are given by

$$\begin{bmatrix} \sigma_{xx} \\ \tau_{xz} \end{bmatrix}^{(k)} = \begin{bmatrix} \bar{C}_{11} & 0 \\ 0 & \bar{C}_{55} \end{bmatrix}^{(k)} \begin{bmatrix} \varepsilon_{xx} \\ \gamma_{xz} \end{bmatrix}^{(k)}, \quad \text{i.e.} \quad \boldsymbol{\sigma}^{(k)} = \bar{\mathbf{C}}^{(k)} \boldsymbol{\varepsilon}^{(k)} \tag{1}$$

where $\boldsymbol{\sigma}^{(k)}$ is stress vector, $\boldsymbol{\varepsilon}^{(k)}$ is the strain vector, and the constitutive one-dimensional laws are given by the elastic stiffness matrix $\bar{\mathbf{C}}^{(k)}$ for the kth layer.

Taking into account the classical assumption of negligible transverse normal stress ($\sigma_{zz}^{(k)} = \sigma_{yy}^{(k)} = 0$), the longitudinal modulus is expressed from the three dimensional constitutive laws by

$$\bar{C}_{11}^{(k)} = C_{11}^{(k)} - 2(C_{12}^{(k)})^2/(C_{23}^{(k)} + C_{33}^{(k)}) \tag{2}$$

where C_{ij} are orthotropic three-dimensional elastic moduli [56].

The transverse shear stress modulus is given by

$$\bar{C}_{55}^{(k)} = C_{55}^{(k)} = G_{xz}^{(k)} \tag{3}$$

The general weak form of the boundary value problem for the beam shown in Fig. 1, considering Eq. (1) and a virtual displacement vector $\delta\mathbf{u}$, is given by the classical virtual work expression

$$\int_V (\delta\boldsymbol{\varepsilon}^{(k)})^T \boldsymbol{\sigma}^{(k)}(\mathbf{u})\, dV - \int_V (\delta\mathbf{u})^T \mathbf{g}\, dV - \int_{\partial V_F} (\delta\mathbf{u})^T \mathbf{F}\, d\partial V = 0 \tag{4}$$

where $\mathbf{g}$ and $\mathbf{F}$ are, respectively, the prescribed body and surface forces applied on ∂V, $\delta\boldsymbol{\varepsilon}^{(k)} = \nabla^{s(k)}(\delta\mathbf{u})$ is the virtual strain, ∇^s denotes symmetric gradient and $(*)^T$ denotes the corresponding transpose.

Substituting Eq. (1) into the weak form of the boundary value problem, Eq. (4) results:

$$\int_V (\delta\boldsymbol{\varepsilon}^{(k)})^T \bar{\mathbf{C}}^{(k)} \boldsymbol{\varepsilon}^{(k)}\, dV - \int_V (\delta\mathbf{u})^T \mathbf{g}\, dV - \int_{\partial V_F} (\delta\mathbf{u})^T \mathbf{F}\, d\partial V = 0 \tag{5}$$

Eq. (5) will be used in Section 4 as the starting point for the proposed hierarchical finite element approximations.

3. Bases of the refined zigzag theory

The kinematics of the refined zigzag theory (RZT) proposed by Tessler et al. [43–45] are essentially those of FDT enhanced by an axial zigzag displacement function $\bar{u}^{(k)}(x,z)$ (Fig. 2), which results of a zig-zag field $\psi(x)$ multiplied by a piecewise continuous transverse function $\phi^{(k)}(z)$, as follows

$$\begin{aligned} u^{(k)}(x,z) &= u_0(x) - z\theta(x) + \bar{u}^{(k)}(x,z) \\ w(x,z) &= w_0(x) \end{aligned} \tag{6}$$

where

$$\bar{u}^{(k)}(x,z) = \phi^{(k)}(z)\psi(x) \tag{7}$$

The key attributes of RZT are, first, the zigzag function vanishes at the top and bottom surfaces of the beam and does not require full shear-stress continuity across the laminated-beam depth. Second, all boundary conditions, including the fully clamped condition, can be modeled adequately. And third, the theory requires only C^0-continuous kinematics for finite element modeling. Overall, the theory appears as a natural extension of Timoshenko theory to laminated composite beams.

Within each layer the zigzag function, depicted in Fig. 1(a), is expressed as

$$\phi^{(k)} = \frac{1}{2}\left(1 - \zeta^{(k)}\right)\bar{\phi}^{(k-1)} + \frac{1}{2}\left(1 + \zeta^{(k)}\right)\bar{\phi}^{(k)} \tag{8}$$

where $\bar{\phi}^{(k-1)}$ and $\bar{\phi}^{(k)}$ are the zigzag function values of $(k-1)$ and (k) interfaces respectively, being $\bar{\phi}^{(0)} = \bar{\phi}^{(N_l)} = 0$, and $\zeta^{(k)} = 2(z - z^{(k-1)})/h^{(k)} - 1$.

The zigzag slope $d\phi^{(k)}/dz$, is denoted by $\beta^{(k)}$ and it is computed from Eq. (8) as

$$\beta^{(k)} = \frac{\bar{\phi}^{(k)} - \bar{\phi}^{(k-1)}}{h^{(k)}} \tag{9}$$

In this theory the zigzag slope $\beta^{(k)}$ is defined by the difference between the transverse shear rigidity of a layer $G_{xz}^{(k)}$, and the effective transverse shear rigidity G of the entire layup,

$$\beta^{(k)} = \frac{G}{G_{xz}^{(k)}} - 1 \tag{10}$$

being

$$G = A\left[\int\int_A \frac{dA}{G_{xz}^{(k)}}\right]^{-1} = h\left[\sum_{k=1}^{N_l} \frac{h^{(k)}}{G_{xz}^{(k)}}\right]^{-1} \tag{11}$$

Introducing Eqs. (9) and (10) into Eq. (8) the expression for the zigzag function for the RZT is obtained,

$$\begin{aligned} \bar{\phi}^{(k)} &= \beta^{(k)} h^{(k)} + \bar{\phi}^{(k-1)} \quad \text{and} \quad \phi^{(k)} \\ &= \frac{h^{(k)}\beta^{(k)}}{2}(\zeta^{(k)} - 1) + \sum_{i=1}^{k} h^{(i)}\beta^{(i)} \end{aligned} \tag{12}$$

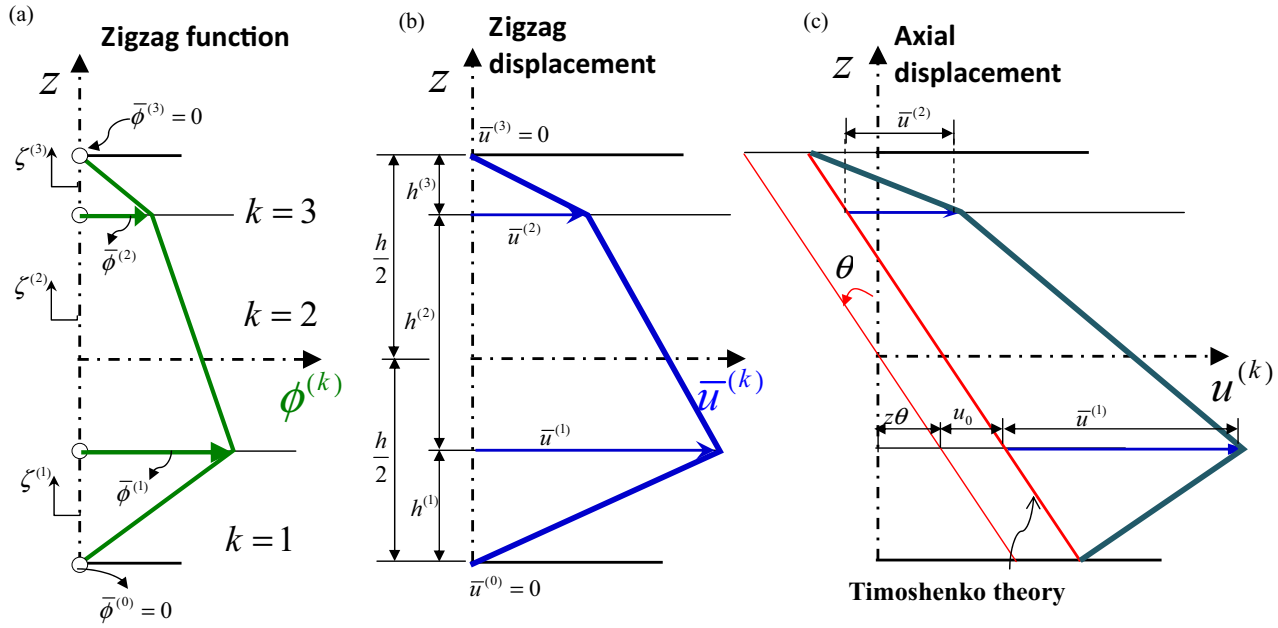

Fig. 2. Schematic representation of the RZT. Thickness distribution of: (a) zigzag function, (b) zigzag displacement, and (c) axial displacement.

Note that RZT theory does not enforce the continuity of the transverse shear stress across the section. This is consistent with kinematic freedom inherent in the lower order kinematic approximation of the underlying beam theory. The reader can obtain a more detailed description of the RZT in Tessler et al. [43–45] and Oñate et al. [42].

4. Hierarchical finite beam element for the refined zigzag theory

4.1. Shape functions

The unknown functions u_0, w, θ and ψ in Eq. (6) are discretized using one finite element according to the hierarchical version of FEM (p-FEM). The natural coordinate $\xi = 2x/L - 1$ is used along the length of the beam, so node 1 corresponds to $\xi = -1$ ($x = 0$) and node 2 corresponds to $\xi = 1$ ($x = L$). The proposed one – dimensional approximation is given by

$$(u_0, w, \theta, \psi) = \sum_{i=1}^{n_u, n_w, n_\theta, n_\psi} N_i(\xi)(c_i^{u_0}, c_i^w, c_i^\theta, c_i^\psi) \tag{13}$$

where $n_*, * = u_0, w, \theta, \psi$ are the number of shape functions; c_i^* are the generalized unknowns displacements used to approximate each kinematic variable and $N_i(\xi)$ are the shape functions.

These shape functions, $N_i(\xi)$, are polynomials expressions and they can be classified in two groups [57], namely: nodal modes for $i = 1, 2$ and internal modes for $i = 3, \ldots, n_*$.

The nodal modes are the classical support local Lagrange polynomials, i.e.:

$$N_i(\xi) = \frac{1}{2}(1 + \xi\xi_i), \quad i = 1, 2 \tag{14}$$

where ξ_i is the local coordinate of the i – th node.

The internal modes are purely local and vanish at the ends of the element (beam). This feature is highly significant since these functions only give additional freedom to the interior of the element. The employment of orthogonal polynomials generated by the Gram-Schmidt recurrence expressions are proposed in this work [58–60]. The first internal mode is obtained as a simpler and lower degree polynomial that satisfies that hierarchical modes contribute only to the internal components of the displacement field of the element, and do not therefore affect to these components at the end nodes. So the first hierarchical (internal) mode results:

$$N_3(\xi) = -1 + \xi^2 \tag{15}$$

This basis polynomial satisfies $N_3(\xi)|_{\xi=-1} = N_3(\xi)|_{\xi=1} = 0$ as required.

The remaining hierarchical modes are obtained by the Gram-Schmidt procedure, starting from the basis polynomial (Eq. (15)), as follows

$$N_4(\xi) = (\xi - B_4)N_3(\xi), \tag{16}$$

$$N_k(\xi) = (\xi - B_k)N_{k-1}(\xi) - C_k N_{k-2}(\xi) \text{ for } k = 5, \ldots, n_{(*)} \tag{17}$$

where

$$B_k = \frac{\int_{-1}^{1} \xi (N_{k-1}(\xi))^2 d\xi}{\int_{-1}^{1} (N_{k-1}(\xi))^2 d\xi}, \quad \text{for} \quad k = 4, \ldots, n_* \tag{18}$$

$$C_k = \frac{\int_{-1}^{1} \xi N_{k-1}(\xi) N_{k-2}(\xi) d\xi}{\int_{-1}^{1} (N_{k-2}(\xi))^2 d\xi}, \quad \text{for} \quad k = 5, \ldots, n_* \tag{19}$$

The coefficients of the polynomials are recomputed so that result orthonormal polynomials:

$$\int_{-1}^{1} (N_k(\xi))^2 d\xi = 1 \tag{20}$$

The application of this procedure ensures that higher-order polynomials (hierarchical modes) satisfy, automatically, the same conditions as the basis polynomial.

Taking into account the features of the nodal and internal modes, the first two generalized displacement unknowns are the values of the kinematic variables at the end nodes, i.e.:$c_1^\alpha = \alpha_1$ and $c_2^\alpha = \alpha_2$, being $\alpha = u_0, w, \theta, \psi$; namely $c_1^u = u_0(\xi = -1) = u_{01}$, $c_2^u = u_0(\xi = 1) = u_{02}$, $c_1^w = w(\xi = -1) = w_{01}$, $c_2^w = w(\xi = 1) = w_{02}$, $c_1^\theta = \theta(\xi = -1) = \theta_1$, $c_2^\theta = \theta(\xi = 1) = \theta_2$, $c_1^\psi = \psi(\xi = -1) = \psi_1$, $c_2^\psi = \psi(\xi = 1) = \psi_2$.

The shape functions N_i, as stated above, are the same for all kinematics variables, however it is possible to use different number of approximation functions for each variable $(n_{u_0}, n_w, n_\theta, n_\psi)$. Finally, Eq. (13) is now written in a matrix form, as follows

$$\mathbf{u} = \begin{Bmatrix} u_0 \\ w \\ \theta \\ \psi \end{Bmatrix} = \begin{Bmatrix} \mathbf{N}_{u_0}\mathbf{c}^{u_0} \\ \mathbf{N}_w\mathbf{c}^w \\ \mathbf{N}_\theta\mathbf{c}^\theta \\ \mathbf{N}_\psi\mathbf{c}^\psi \end{Bmatrix} \tag{21}$$

where

$$\mathbf{N}_\alpha = [N_1, N_2, \ldots, N_{n_\alpha}] \tag{22}$$

$$\mathbf{c}^\alpha = \begin{Bmatrix} c_1^\alpha & c_2^\alpha & \ldots & c_{n_\alpha}^\alpha \end{Bmatrix}^T, \quad \alpha = u_0, w, \theta, \psi \tag{23}$$

Note that the dimensions of $\mathbf{N}_\alpha$ depends on the number of shape functions for each kinematic variable $(n_{u_0}, n_w, n_\theta, n_\psi)$.

4.2. Expression of strains and stress

The strains for the laminated beam (Fig. 1), considering the RZT theory (Fig. 2) given by Eqs. (6) and (7) are:

$$\varepsilon_{xx}^{(k)} = \frac{du_0}{dx} - z\frac{d\theta}{dx} + \phi^{(k)}\frac{d\psi}{dx} \tag{24}$$

$$\gamma_{xz}^{(k)} = \frac{dw}{dx} - \theta + \beta^{(k)}\psi \tag{25}$$

where Eq. (24) contains the axial elongations (du_0/dx), the pseudo-curvature $(d\theta/dx)$ and the derivative of the function zigzag amplitude $(d\psi/dx)$; and in Eq. (25) $dw/dx - \theta$ is the average transverse shear stress of Timoshenko beam theory and $\beta^{(k)}$ is constant across each layer.

Eqs. (24) and (25) can be written as

$$\varepsilon_{xx}^{(k)} = \mathbf{S}_p^{(k)}\boldsymbol{\varepsilon}_p; \quad \gamma_{xz}^{(k)} = \mathbf{S}_t^{(k)}\boldsymbol{\varepsilon}_t \tag{26}$$

where

$$\mathbf{S}_p^{(k)} = [1, -z, \phi^{(k)}]; \quad \boldsymbol{\varepsilon}_p = \left[\frac{du_0}{dx}, \frac{d\theta}{dx}, \frac{d\psi}{dx}\right]^T \tag{27}$$

$$\mathbf{S}_t^{(k)} = [1, -1, \beta^{(k)}]; \quad \boldsymbol{\varepsilon}_t = \left[\frac{dw}{dx}, \theta, \psi\right]^T \tag{28}$$

In Eqs. (27) and (28) $\boldsymbol{\varepsilon}_p$ and $\boldsymbol{\varepsilon}_t$ are, respectively, the generalized in-plane and transverse shear strain vectors, respectively.

Substituting Eq. (13) into the generalized strain vectors (Eqs. (27) and (28)) leads to

$$\boldsymbol{\varepsilon}_p = \begin{Bmatrix} u_{0,x} \\ \theta_{,x} \\ \psi_{,x} \end{Bmatrix} = \begin{Bmatrix} \mathbf{N}_{u_0,x}\mathbf{c}^{u_0} \\ \mathbf{N}_{w,x}\mathbf{c}^\theta \\ \mathbf{N}_{\psi,x}\mathbf{c}^\psi \end{Bmatrix}, \quad \boldsymbol{\varepsilon}_t = \begin{Bmatrix} w_{,x} \\ \theta \\ \psi \end{Bmatrix} = \begin{Bmatrix} \mathbf{N}_{w,x}\mathbf{c}^w \\ \mathbf{N}_\theta\mathbf{c}^\theta \\ \mathbf{N}_\psi\mathbf{c}^\psi \end{Bmatrix} \tag{29}$$

where $\alpha_{,x}$ denotes differentiation with respect to variable x.

The generalized strain vectors of Eq. (29) can be expressed in other way, which will be convenient for obtaining the global finite hierarchical element equation,

$$\boldsymbol{\varepsilon}_p = \mathbf{B}_p\mathbf{c}, \quad \boldsymbol{\varepsilon}_t = \mathbf{B}_t\mathbf{c} \tag{30}$$

where $\mathbf{c}$ contains all generalized nodal and internal displacement unknowns (see Eq. (23)); and $\mathbf{B}_p, \mathbf{B}_t$ are, respectively, the generalized in-plane and transverse shear strain matrices, given by

$$\mathbf{c} = \begin{Bmatrix} \mathbf{c}^{u_0} \\ \mathbf{c}^w \\ \mathbf{c}^\theta \\ \mathbf{c}^\psi \end{Bmatrix}; \quad \mathbf{B}_p = \begin{bmatrix} \mathbf{N}_{u_0,x} & \mathbf{0} & \mathbf{0} & \mathbf{0} \\ \mathbf{0} & \mathbf{0} & \mathbf{N}_{\theta,x} & \mathbf{0} \\ \mathbf{0} & \mathbf{0} & \mathbf{0} & \mathbf{N}_{\psi,x} \end{bmatrix};$$

$$\mathbf{B}_t = \begin{bmatrix} \mathbf{0} & \mathbf{N}_{w,x} & \mathbf{0} & \mathbf{0} \\ \mathbf{0} & \mathbf{0} & \mathbf{N}_\theta & \mathbf{0} \\ \mathbf{0} & \mathbf{0} & \mathbf{0} & \mathbf{N}_\psi \end{bmatrix} \tag{31}$$

Replacing Eq. (29) into Eqs. (1) the following stress expressions for the kth layer are obtained

$$\sigma_{xx}^{(k)} = \bar{C}_{11}^{(k)}\mathbf{S}_p^{(k)}\boldsymbol{\varepsilon}_p = \bar{C}_{11}^{(k)}\mathbf{S}_p^{(k)}\mathbf{B}_p\mathbf{c} \tag{32}$$

$$\tau_{xz}^{(k)} = \bar{C}_{55}^{(k)}\mathbf{S}_t^{(k)}\boldsymbol{\varepsilon}_t = \bar{C}_{55}^{(k)}\mathbf{S}_t^{(k)}\mathbf{B}_t\mathbf{c} \tag{33}$$

4.3. Expression of virtual work

The virtual work expression for a distributed transverse load $q(x)$, is obtained replacing Eq. (26) into Eq. (5) and integrating the cross sectional area A, as follows

$$\int_L [\delta\boldsymbol{\varepsilon}_p^T\mathbf{D}^p\boldsymbol{\varepsilon}_p + \delta\boldsymbol{\varepsilon}_t^T\mathbf{D}^t\boldsymbol{\varepsilon}_t]\,dx - \int_L \delta w\, q\, dx = 0 \tag{34}$$

where the generalized constitutive matrices $\mathbf{D}^p$ and $\mathbf{D}^t$ are given by

$$\mathbf{D}^p = \int\int_A \bar{C}_{11}^{(k)}\mathbf{S}_p^{(k)T}\mathbf{S}_p^{(k)}dA = \int\int_A \bar{C}_{11}^{(k)}\begin{bmatrix} 1 & -z & \phi^{(k)} \\ & z^2 & -z\phi^{(k)} \\ sym & & (\phi^{(k)})^2 \end{bmatrix}dA \tag{35}$$

$$\mathbf{D}^t = \int\int_A \bar{C}_{55}^{(k)}\mathbf{S}_t^{(k)T}\mathbf{S}_t^{(k)}dA = \int\int_A \bar{C}_{55}^{(k)}\begin{bmatrix} 1 & -1 & \beta^{(k)} \\ & 1 & -\beta^{(k)} \\ sym & & (\beta^{(k)})^2 \end{bmatrix}dA \tag{36}$$

From Eqs. (21) and (29), the virtual displacement and generalized strain fields are expressed in terms of the virtual nodal modes and internal modes of the kinematic variables,

$$\delta\mathbf{u} = \begin{Bmatrix} \mathbf{N}_{u_0}\delta\mathbf{c}^{u_0} \\ \mathbf{N}_w\delta\mathbf{c}^w \\ \mathbf{N}_\theta\delta\mathbf{c}^\theta \\ \mathbf{N}_\psi\delta\mathbf{c}^\psi \end{Bmatrix}, \quad \delta\boldsymbol{\varepsilon}_p = \mathbf{B}_p\delta\mathbf{c}, \quad \delta\boldsymbol{\varepsilon}_t = \mathbf{B}_t\delta\mathbf{c} \tag{37}$$

The discretized equilibrium equations are obtained by substituting Eqs. (30) and (37) into the virtual work expression (Eq. (34)). After simplification of the virtual generalized kinetic unknowns, we obtain

$$\int_{-1}^{1}(\mathbf{B}_p^T\mathbf{D}^p\mathbf{B}_p + \mathbf{B}_t^T\mathbf{D}^t\mathbf{B}_t)\mathbf{c}\,d\xi - \int_{-1}^{1}\mathbf{B}_f\, q\; d\xi = \mathbf{0} \tag{38}$$

where $\mathbf{B}_f = [\mathbf{0}_{1\times n_u}, \mathbf{N}_w, \mathbf{0}_{1\times n_\theta}, \mathbf{0}_{1\times n_\psi}]^T$

Expression (38) can be finally expressed in the following classical matrix equation as:

$$\mathbf{K}\mathbf{c} - \mathbf{f} = \mathbf{0} \tag{39}$$

The stiffness matrix $\mathbf{K}$ is the global matrix for the hierarchical finite element, and it is given by

$$\mathbf{K} = \int_{-1}^{1}\mathbf{B}^T\mathbf{D}\mathbf{B}d\xi \tag{40}$$

where

$$\mathbf{B}^T = [\mathbf{B}_p^T, \mathbf{B}_t^T], \quad \mathbf{D} = \begin{bmatrix} \mathbf{D}^p & \mathbf{0}_{3\times3} \\ \mathbf{0}_{3\times3} & \mathbf{D}^t \end{bmatrix} \tag{41}$$

The equivalent force vector $\mathbf{f}$ results:

$$\mathbf{f} = [\mathbf{0}_{1\times n_u}, \mathbf{f}^w, \mathbf{0}_{1\times n_\theta}, \mathbf{0}_{1\times n_\psi}]^T \tag{42}$$

where $f_i^w = \int_{-1}^{1} qN_i d\xi$, $i = 1, n_w$

The stiffness matrix $\mathbf{K}$ in Eq. (40), can be easily expressed as follows:

$$\mathbf{K} = \begin{bmatrix} \mathbf{k}^{uu} & \mathbf{0} & \mathbf{k}^{u\theta} & \mathbf{k}^{u\psi} \\ & \mathbf{k}^{ww} & \mathbf{k}^{w\theta} & \mathbf{k}^{w\psi} \\ & & \mathbf{k}^{\theta\theta} & \mathbf{k}^{\theta\psi} \\ sym & & & \mathbf{k}^{\psi\psi} \end{bmatrix} \tag{43}$$

where their respective components are:

$$\begin{aligned}
k_{ij}^{uu} &= D_{11}^{p} \tfrac{4}{L^2} \int_{-1}^{1} \tfrac{dN_i}{d\xi} \tfrac{dN_j}{d\xi} d\xi, \quad i = 1, n_u; \quad j = 1, n_u \\
k_{ij}^{u\theta} &= D_{12}^{p} \tfrac{4}{L^2} \int_{-1}^{1} \tfrac{dN_i}{d\xi} \tfrac{dN_j}{d\xi} d\xi, \quad i = 1, n_u; \quad j = 1, n_\theta \\
k_{ij}^{u\psi} &= D_{13}^{p} \tfrac{4}{L^2} \int_{-1}^{1} \tfrac{dN_i}{d\xi} \tfrac{dN_j}{d\xi} d\xi, \quad i = 1, n_u; \quad j = 1, n_\psi \\
k_{ij}^{ww} &= D_{11}^{t} \tfrac{4}{L^2} \int_{-1}^{1} \tfrac{dN_i}{d\xi} \tfrac{dN_j}{d\xi} d\xi, \quad i = 1, n_w; \quad j = 1, n_w \\
k_{ij}^{w\theta} &= D_{12}^{t} \tfrac{2}{L} \int_{-1}^{1} \tfrac{dN_i}{d\xi} N_j d\xi, \quad i = 1, n_w; \quad j = 1, n_\theta \\
k_{ij}^{w\psi} &= D_{13}^{t} \tfrac{2}{L} \int_{-1}^{1} \tfrac{dN_i}{d\xi} N_j d\xi, \quad i = 1, n_w; \quad j = 1, n_\psi \\
k_{ij}^{\theta\theta} &= D_{22}^{p} \tfrac{4}{L^2} \int_{-1}^{1} \tfrac{dN_i}{d\xi} \tfrac{dN_j}{d\xi} d\xi + D_{22}^{t} \int_{-1}^{1} N_i N_j d\xi, \quad i = 1, n_\theta; \quad j = 1, n_\theta \\
k_{ij}^{\theta\psi} &= D_{23}^{p} \tfrac{4}{L^2} \int_{-1}^{1} \tfrac{dN_i}{d\xi} \tfrac{dN_j}{d\xi} d\xi + D_{23}^{t} \int_{-1}^{1} N_i N_j d\xi, \quad i = 1, n_\theta; \quad j = 1, n_\psi \\
k_{ij}^{\psi\psi} &= D_{33}^{p} \tfrac{4}{L^2} \int_{-1}^{1} \tfrac{dN_i}{d\xi} \tfrac{dN_j}{d\xi} d\xi + D_{33}^{t} \int_{-1}^{1} N_i N_j d\xi, \quad i = 1, n_\psi; \quad j = 1, n_\psi
\end{aligned} \tag{44}$$

The new hierarchical beam finite element based on RZT Tessler developments is termed PRZ. Studies of shear locking, convergence and validations are presented in the next sections.

5. Study shear locking for PRZ element

Shear locking is due to the inability of shear deformable elements to accurately model the bending within an element under a state of zero transverse shearing strain. When thin beams are analyzed by the shear deformable elements, the energy due to transverse shear strains must vanish. Numerically this is equivalent to requiring the product of the shear stiffness matrix and the displacement vector be zero. Therefore, in order to obtain a non-trivial solution, the shear stiffness matrix must be singular. One way to achieve the singularity of the transverse shear stiffness matrix is to use an order of numerical integration lower than is necessary to evaluate the integrals exactly. This procedure, i.e., reduced integration of transverse shear stiffnesses has been adopted by Oñate et al. [42] for overcoming the shear locking problem in their linear two-noded beam element based on RZT. P-version of FEM is much less prone of shear locking because of the increase of the number of terms in the enrichment basis functions, i. e., *p*-refinement. Moreover, it was theoretically and numerically shown, that the *p*-version is free of locking effects, if the polynomial degree is chosen to be moderately high.

In order to show that the new PRZ element is free of shear locking, the performance of this element in the analysis of a cantilever beam of length L under an end point load of value $F = 1$ (Fig. 3a) is presented. For the clamped end all the nodal degrees of freedoms at the boundary are fully restrained ($u_0 = w = \theta = \psi = 0$ at $x = 0$), while for the free end all the nodal degrees of freedoms are unrestrained. The material properties correspond to that designated as Composite B in Table 1.

Beams with different length-to-thickness ratios λ (with $\lambda = L/h$), from thick to thin beams, are analyzed using 8 (eight) Gram Schmidt (GS) polynomials for each kinematic variable. To this study, firstly, the free end deflection is analyzed and the following dimensionless variable is used:

$$\bar{w}|_{x=L} = \frac{w\bar{E}}{10F\lambda^3} \tag{45}$$

where $\bar{E} = \frac{1}{N_l}\sum_{k=1}^{N_l} E^{(k)}$

Fig. 4 shows the variation of the dimensionless free end deflection against λ. The graph shows that the solution converges as the length-to-thickness ratio of the beam increases, tending towards a horizontal asymptote corresponding to the thin beam deflection with equivalent material properties. It is clear that the proposed PRZ element is free of shear locking and from $\lambda \geqslant 60$ the solution tends stably to the corresponding solution for thin beams.

Second, to verify that the PRZ element is free from locking shear, transverse shear stresses are determined both from the constitutive relations (Eq. (33)) as well as from the equilibrium equation at the post-processing level i.e.,

$$\tau_{xz}^{(k)}(z) = -\int_{-h/2}^{z} \frac{\partial \sigma_{xx}^{(k)}}{\partial x} dz \tag{46}$$

The determination is made for a thick beam ($\lambda = 5$) and for a thin beam ($\lambda = 100$), taking two different sections along the beam. Figs. 5 and 6 show the thickness distribution of shear stresses τ_{xz} in sections located at distances $L/20$ and $3L/4$ from the clamped end. The transverse shear stresses computed from the constitutive relations are labeled as "Present-const", while the shear stresses computed from the equilibrium equations are labeled as "Present-equil". For comparison purpose two τ_{xz} profiles obtained by Oñate et al. [42] have been included in the figures. One of these results were obtained using a mesh of 27,000 four-noded plane stress rectangles (labeled as "PS") and the other were obtained with 100 linear two-noded beam elements and reduced integration proposed by the mentioned authors (labeled as "RI").

An examination of the numerical results presented in these figures shows that the hierarchical finite element developed with equal interpolation of all generalized displacements does not experience shear locking. The element behaves uniformly well for thin and thick beams. The finite element results are in excellent agreement with those reported in Ref. [42] where reduced integration has been used. The displacements converge faster than stresses, which is expected because the rate of convergence of gradients of the solution is one order less than the rate of convergence of the solution.

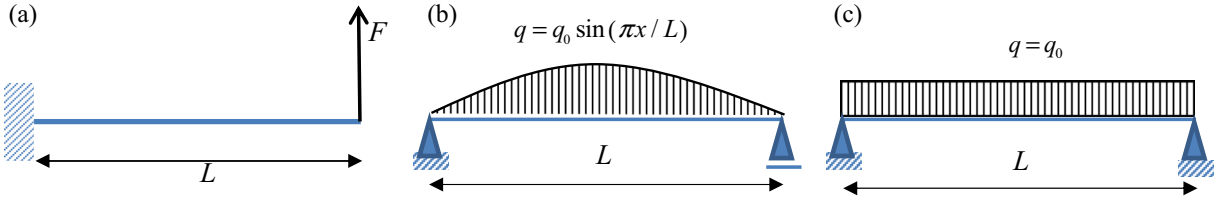

Fig. 3. Structural representation of the analyzed beams; (a) Cantilever beam under a free end point load, (b) Simple supported beam under sinusoidal load, (c) Simple supported beam under uniform load.

Table 1
Material properties of 3-layered symmetric and non-symmetric laminates.

Composite		Material Properties		
		Layer 1 (bottom)	Layer 2 (core)	Layer 3 (top)
(A) Non-Symmetric laminate	$h^{(k)}$ [mm]	6.66	6.66	6.66
	$E^{(k)}$ [MPa]	4.40E + 05	2.19E + 04	2.19E + 05
	$G_{xz}^{(k)}$ [MPa]	2.00E + 05	8.80E + 03	8.76E + 04
(B) Symmetric laminate	$h^{(k)}$ [mm]	6.66	6.66	6.66
	$E^{(k)}$ [MPa]	2.19E5	2.19E3	2.19E5
	$G_{xz}^{(k)}$ [MPa]	8.76E4	8.80E2	8.76E4
(C) Non-symmetric laminate	$h^{(k)}$ [mm]	2	16	2
	$E^{(k)}$ [MPa]	7.30E5	7.30E2	2.19E5
	$G_{xz}^{(k)}$ [MPa]	2.92E5	2.90E2	8.76E4
(D) Non-symmetric laminate	$h^{(k)}$ [mm]	6.6666	6.6666	6.6666
	$E^{(k)}$ [MPa]	2.19E5	5.30E5	7.30E5
	$G_{xz}^{(k)}$ [MPa]	8.76E4	2.90E2	2.92E2

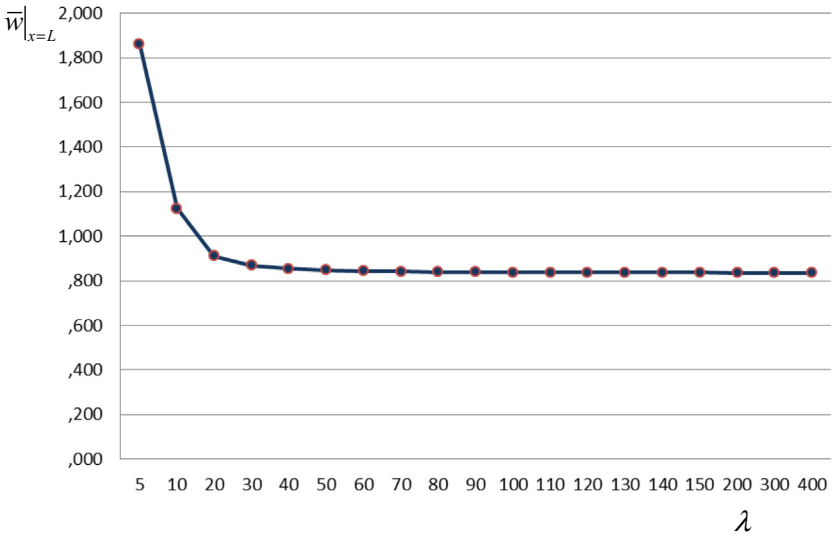

Fig. 4. Free end deflection $\bar{w}$ for a laminated cantilever beam (Composite B) for different length – to – thickness ratios.

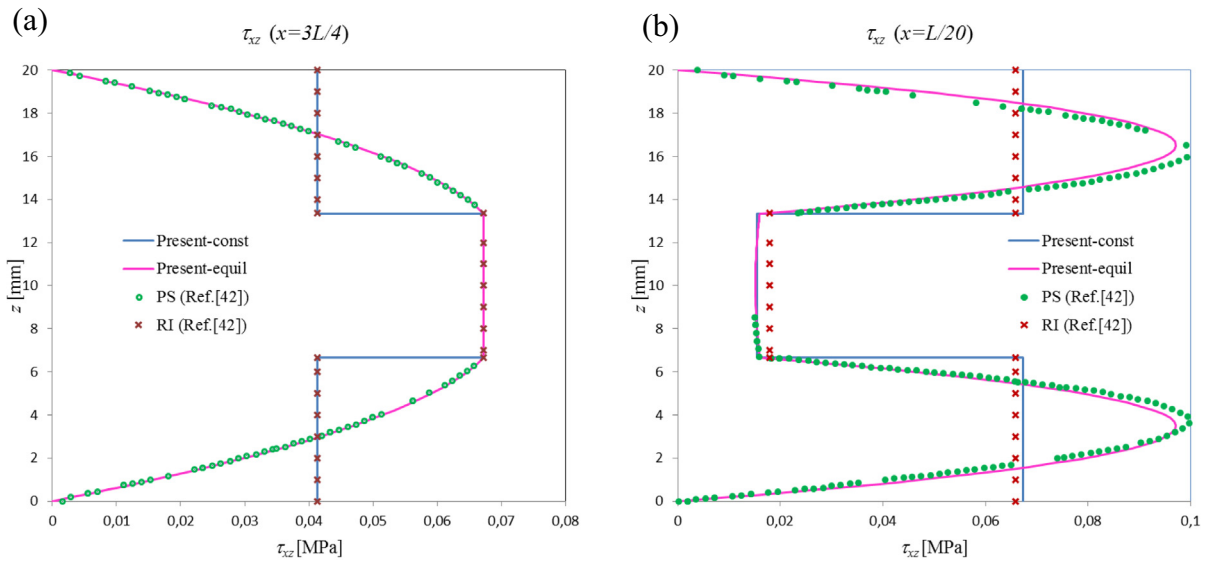

Fig. 5. Symmetric (composite B) cantilever thick beam ($\lambda = 5$) under end point load. Thickness distribution of shear stress at different sections.

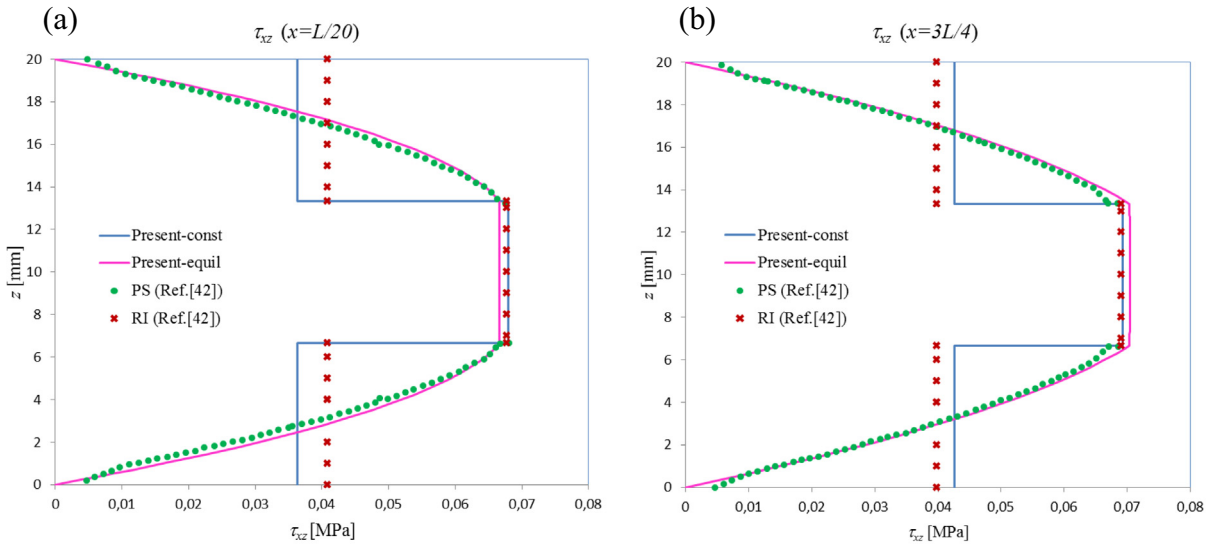

Fig. 6. Symmetric (composite B) cantilever thin beam ($\lambda = 100$) under end point load. Thickness distribution of shear stress at different sections.

For very thin beams, very good agreement is found between the thin- theory values and those from RZT beam theory employing PRZ elements, showing that the proposed element is not prone to shear locking.

6. Convergence analysis

Recall that the advantages of the *p*-version of FEM are not limited to the greater convergence rate. In fact, with *h* methods, the accuracy of the solution is determined by executing several analyses with different meshes, an expensive and time-consuming process, both because of the computational cost and because of the operator time required to define the different models. In *p*-convergent approximations, the number of finite elements is determined by the geometry and is small. Moreover, to verify the results, the order of the approximation can be selectively increased. This operation is carried out very efficiently because it is not necessary to generate a new mesh and because the new linear stiffness matrices contain the preceding ones [55].

For the convergence study once again the cantilever beam subjected to a unit load at the free end is analyzed (Fig. 3a). Displacements and stresses at different points of symmetric (Composite B, Table 1) and arbitrarily laminated (Composite A and C, Table 1) beams are obtained. For both materials, length-to-thickness ratios, $\lambda = 5, 10$, are considered. For the different combinations of length-to-thickness ratios and material properties, convergence studies are performed by varying the amount of GS orthogonal polynomials of the approximation functions for the four kinematic variables, from 1 to 10.

Tables 2–5 show, respectively, the variation of the transverse deflection w and the amplitude of ψ function at the beam free end; the maximum normal stress σ_{xx} at the clamped end and the maximum transverse shear stress τ_{xz} at the central section of the beam, as the number of polynomials enrichment (Gram-Schmidt polynomials) is increased. Also, the transverse deflections$w$, for symmetric (comp. B) and non-symmetric (comp. C) laminated beams with length – to – thickness ratio $\lambda = 5$, are plotted against the number of GS enrichment polynomials in Fig. 7.

In Tables 2–5 the convergence is quantified through the relative error given by the following expression

$$e_r = \left| \frac{\upsilon_{10} - \upsilon_i}{\upsilon_{10}} \right| \tag{47}$$

where υ_{10} and y υ_i are the numerical values of the different magnitudes obtained employing 10 GS polynomials and $i\,(i = 1, \ldots, 10)$ GS polynomials, respectively.

The analysis of the results showed in Tables 2–5 and Fig. 7 demonstrates that the numerical solutions are convergent for transverse displacement w, amplitude of zigzag function ψ and also for normal (σ_{xx}) and transverse shear (τ_{xz}) stresses in which the derivatives of the displacement field components are involved. As expected, convergence is slower in the case of Composite C (more heterogeneous material) than for composite B. For 8 GS enrichment polynomials errors for all considered magnitudes are less than 0.5% for composites A, B and C, the only exception is the value of the normal stress σ_{xx} for composite C, in this case the error is less than 1.8%. For these reasons, the calculations using eight GS enrichment polynomials for each kinematic variable, is considered sufficient to obtain good accuracy.

7. Validation and numerical examples

In this section different problems of laminated beams are solved to show the accuracy and applicability of the present FE hierarchical model under static loading. In all the examples presented, both in this section and in the next, the beams are modeled with a single finite element with two end nodes, coincident with the ends of the analyzed beams. The internal or hierarchical nodes depend on the number of GS polynomials used in each case and are obtained automatically (see Eqs. (39)–(43)).

7.1. Symmetric and antisymmetric cross-ply laminated beams

In this subsection results obtained for symmetric (0°/90°/0°) and antisymmetric (0°/90°) cross-ply laminated beams constituted by orthotropic material are presented. All layers in the laminates have the same thickness ($h^{(k)} = h/N_l$), and their material properties are:$E_1 = 172.4$ GPa, $E_2 = 6.895$ GPa, $G_{12} = 3.448$ GPa, $G_{23} = 1.379$ GPa, $\nu_{12} = \nu_{23} = 0.25$, where subscripts 1 and 2 refer, respectively, to the fiber direction and to the normal direction.

The symmetric and antisymmetric beams are simply supported and they are subjected to a sinusoidal load $q = q_0 \sin(\pi x/L)$, as

Table 2
Convergence study of three layered symmetric and non-symmetric cantilever thick beams. Relative error for w at $x = L$ for increasing number of GS polynomials.

Composites						
	A		B		C	
$\lambda = L/h$	5	10	5	10	5	10
$e_r(\%)-w(x = L)$						
1	13.961	19.044	14.390	15.734	17.446	17.104
2	0.576	0.226	1.161	1.019	4.151	3.918
3	0.168	0.102	0.138	0.271	1.088	1.533
4	0.040	0.043	0.010	0.058	0.232	0.585
5	0.008	0.017	0.001	0.009	0.038	0.203
6	0.001	0.006	0.000	0.001	0.005	0.062
7	0.000	0.002	0.000	0.000	0.001	0.016
8	0.000	0.000	0.000	0.000	0.000	0.004
9	0.000	0.000	0.000	0.000	0.000	0.001
10	0.000	0.000	0.000	0.000	0.000	0.000

Table 3
Convergence study of three layered symmetric and non-symmetric cantilever thick beams. Relative error for ψ at $x = L$ for increasing number of GS polynomials.

Composites						
	A		B		C	
$\lambda = L/h$	5	10	5	10	5	10
$e_r(\%)-\psi(x = L)$						
1	100.372	194.748	45.084	95.026	17.446	49.393
2	8.942	2.563	6.516	14.863	4.151	20.340
3	4.214	5.082	0.870	5.662	1.088	7.196
4	1.306	3.913	0.070	1.445	0.232	1.793
5	0.290	2.178	0.004	0.263	0.038	0.324
6	0.049	0.945	0.000	0.036	0.005	0.044
7	0.006	0.348	0.000	0.004	0.001	0.005
8	0.001	0.098	0.000	0.000	0.000	0.000
9	0.000	0.033	0.000	0.000	0.000	0.000
10	0.000	0.000	0.000	0.000	0.000	0.000

Table 4
Convergence study of three layered symmetric and non-symmetric cantilever thick beams. Relative error for $(\sigma_{xx})_{\max}$ at $x = 0$ for increasing number of GS polynomials.

Composites						
	A		B		C	
$\lambda = L/h$	5	10	5	10	5	10
$e_r(\%)-(\sigma_{xx})_{\max}(x = 0)$						
1	99.924	45.979	43.141	42.285	69.413	64.480
2	17.108	12.346	18.176	18.403	50.243	51.041
3	11.051	9.952	7.225	11.445	32.314	40.928
4	6.091	7.484	0.499	5.972	17.253	30.229
5	2.843	5.167	0.499	2.600	7.638	20.146
6	1.139	3.224	0.097	0.963	2.869	11.941
7	0.397	1.785	0.016	0.309	0.933	6.217
8	0.119	0.843	0.002	0.085	0.261	1.752
9	0.027	0.292	0.000	0.018	0.056	0.896
10	0.000	0.000	0.000	0.000	0.000	0.000

shown in Fig. 3b. For these support conditions only three degrees of freedoms are restrained: $w(x = 0)$, $w(x = L)$ and $u_0(x = 0)$. The obtained results, expressed in non-dimensional form, are shown in Tables 6 and 7 for several values of length-to-thickness ratios ($\lambda = L/h$). Mid-span deflections and the normal (at$(L/2, -h/2)$) and transverse shear at $\tau_{xz}(0, -h/4)$ stresses for 0°/90° antisymmetric laminated beams are presented in Table 6; and mid-span deflections and the normal (at $(L/2, h/2)$) and transverse shear at $\tau_{xz}(0, 0)$ stresses for 0°/90°/0° symmetric laminated beams are depicted in Table 7. Results in Tables 6 and 7 are compared with the 3D elasticity solution by Pagano [46] and with those published by Vidal and Polit [40]. Even though the 3D elasticity solution by Pagano was developed for cylindrical bending of an infinitely wide plate, the solution is equally applicable to beams under plane strain. These tables prove again the good performance of the PRZ p-FEM model for transverse deflections, and for normal and transverse stresses in both cases, symmetric and antisymmetric cross-ply laminates. Results are in good agreement with respect to the reference solutions and it is seen from these tables that the element performs quite well for thick beams as well as thin beams, as has been previously remarked (Section 5).

7.2. Three layered thick cantilever beam under end point load, with non-symmetric material properties

Three-layered thick cantilever beam (Fig. 3a), with mid plane non-symmetric material properties (Composite C), is considered in this subsection. In this sandwich laminate the core is eight times thicker than the face sheets and is three orders of magnitude more compliant than the bottom face sheet. Figs. 5–10 show different

Table 5
Convergence study of three layered symmetric and non-symmetric cantilever thick beams. Relative error for $(\tau_{xz})_{max}$ at $x = L/2$ for increasing number of GS polynomials.

Composites						
	A		B		C	
$\lambda = L/h$	5	10	5	10	5	10
$e_r(\%) - (\tau_{xz})_{max}(x = L/2)$						
1	99.991	95.894	33.693	53.549	176.151	35.364
2	8.925	10.899	2.814	8.625	44.083	13.875
3	4.115	3.166	2.422	5.496	9.007	8.638
4	1.797	4.317	0.180	1.336	1.336	4.114
5	0.942	2.105	0.116	1.022	1.243	3.550
6	0.248	1.353	0.005	0.136	0.134	1.063
7	0.119	0.707	0.003	0.103	0.127	1.013
8	0.024	0.458	0.000	0.010	0.009	0.264
9	0.011	0.288	0.000	0.007	0.009	0.256
10	0.000	0.000	0.000	0.000	0.000	0.000

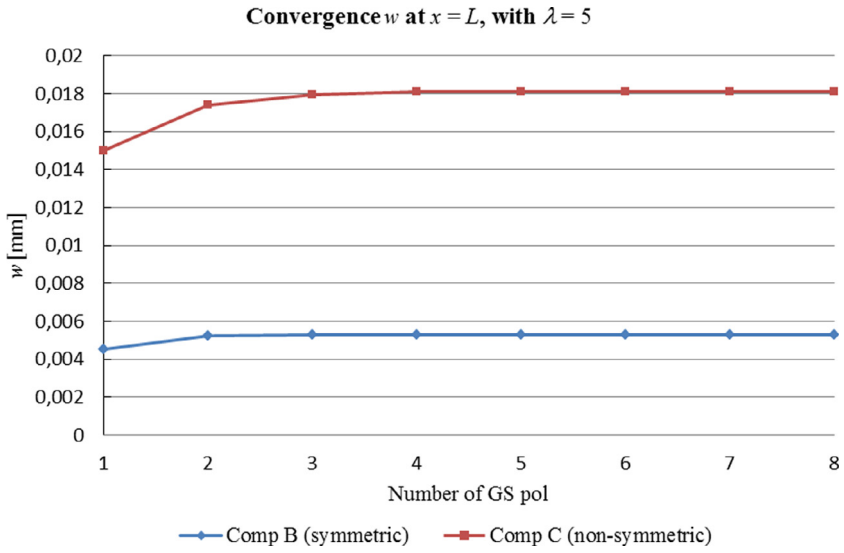

Fig. 7. Transverse free end deflection w for different layer sequence: convergence study for $\lambda = 5$.

Table 6
Non-dimensional displacements and stresses of antisymmetric 0°/90° cross-ply beam under sinusoidal load for different values of λ.

λ	4	6	8	10	20	40	100
$100w(L/2)E_2h^3/q_0L^4$							
Present (PRZ)	4.5137	3.4687	3.1006	2.9298	2.7014	2.6442	2.6282
Ref. [40]	4.5438	–	–	–	2.7036	2.6450	–
Ref. [46]	4.7076	3.5600	3.1504	2.9596	2.7092	2.6462	2.6220
$\sigma_{xx}(L/2, -h/2)/q_0$							
Present (PRZ)	26.748	61.490	110.27	173.03	696.22	2789.2	17439.7
Ref. [40]	31.8	–	–	–	703.6	2803.1	–
Ref. [46]	30.0	65.382	114.18	176.95	699.7	2792.6	17443.7
$\tau_{xz}(0, -h/4)/q_0$							
Present (PRZ)	2.8396	4.3315	5.8146	7.2926	14.653	29.341	73.378
Ref. [40]	2.843	–	–	–	14.574	29.174	–
Ref. [46]	2.706	4.2532	5.7528	7.2419	14.620	29.325	73.373

mechanical responses of this three-layered thick cantilever beam obtained applying PRZ present approach. Also, these figures include plane stress results reported in [42], where legend caption PS denotes these reference solutions obtained with meshes of 27,000 four-noded plane stress quadrilaterals.

Fig. 8 shows the transverse deflection along the beam length. Fig. 9 shows the distribution of the axial displacements at the upper (Fig. 9a) and lower (Fig. 9b) surfaces of layer 3 (top layer) along the beam length. Fig. 10 shows the thickness distribution for the axial displacement at sections located at distances $L/2$ (Fig. 10a) and $3L/4$ (Fig. 10b) from the clamped end. All displacements along x axis, both transverse and axial, and in the last case also along the thickness, obtained using 8 GS enrichment functions for each kinematic variable, are in very good agreement with the plane stress reference solution. Figs. 11 and 12 show the thickness distribution for the axial stress σ_{xx} at the clamped section and the center of the beam, respectively. PRZ results agree very well with those of the reference solution for both sections, namely at $x = 0$

Table 7
Non-dimensional displacements and stresses of symmetric 0°/90°/0° cross-ply beam under sinusoidal load for different values of λ.

λ	4	6	8	10	20	40	100
$100w(L/2)E_2h^3/q_0L^4$							
Present (PRZ)	2.8031	1.5898	1.1329	0.9139	0.6134	0.5366	0.5150
Ref. [40]	2.8027	–	–	–	0.6151	0.5371	–
Ref. [46]	2.8899	1.6345	1.1598	0.9316	0.6185	0.5379	0.5139
$\sigma_{xx}(L/2,h/2)/q_0$							
Present (PRZ)	16.195	29.968	48.138	71.097	260.59	1017.1	6311.97
Ref. [40]	19.5	–	–	–	265.4	1024.4	–
Ref. [46]	18.809	32.531	50.704	73.672	263.2	1019.7	6314.58
$\tau_{xz}(0,0)/q_0$							
Present (PRZ)	1.4358	2.3890	3.3255	4.2467	8.7530	17.644	44.207
Ref. [40]	1.4202	–	–	–	8.6988	17.5400	–
Ref. [46]	1.4318	2.3805	3.3167	4.2385	8.7483	17.641	44.206

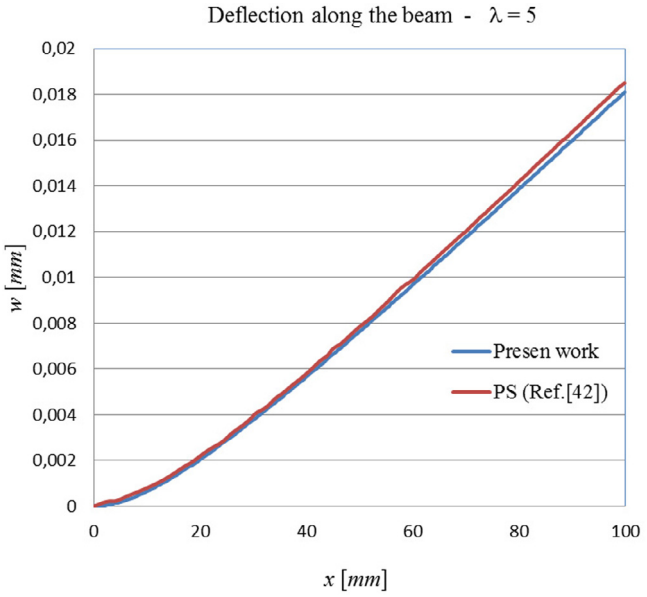

Fig. 8. Transverse deflection of non-symmetric (composite C) cantilever thick beam under end point load ($\lambda = 5$).

and $x = L/2$. Fig. 13 shows the thickness distribution for the transverse shear stress τ_{xz} at different sections (Fig. 13a, at $x = L/4$ and Fig. 13b at $x = 3L/4$). It is observed that the proposed approach provide an accurate estimate of the average transverse shear stress, for each layer, if computed from the constitutive relations ("Present-const" in Fig. 13); however, the distribution of the shear stress can be computed from the equilibrium equations ("Present-equil" in Fig. 13) showing an excellent agreement with the reference solution.

7.3. Three-layered simple supported thick beam under uniform load

The next example analyzes the behavior of a three layered simply supported beam (Fig. 3c) under a uniformly distributed load of unit value ($q = 1$) and span to thickness ratio $\lambda = 5$. In this case the degrees of freedoms u_0 and w are restrained at both beam ends ($x = 0, L$), unlike the beam shown in Fig. 3b.

The material properties and the thickness for the three layers are given in Table 1 (Composite D). As composite C, this material has a non-symmetric layer distribution with respect to the beam axis. The results obtained employing the proposed PRZ formulation shown in Figs. 14–16 are compared, in some cases, with solutions provided by Oñate et al. [42]. As in Section 7.2 results obtained with PRZ element have been labeled as "Present" and, for the case

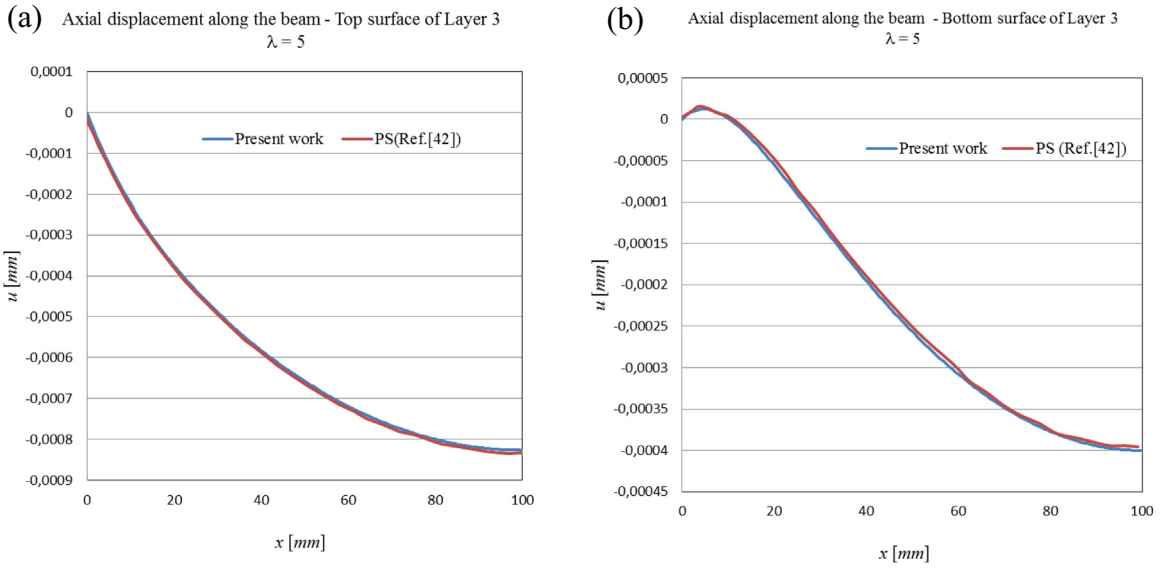

Fig. 9. Non symmetric (composite C) cantilever thick beam ($\lambda = 5$) under end point load. Axial displacements (a) at the upper surface and (b) at the lower surface of layer 3 (top layer).

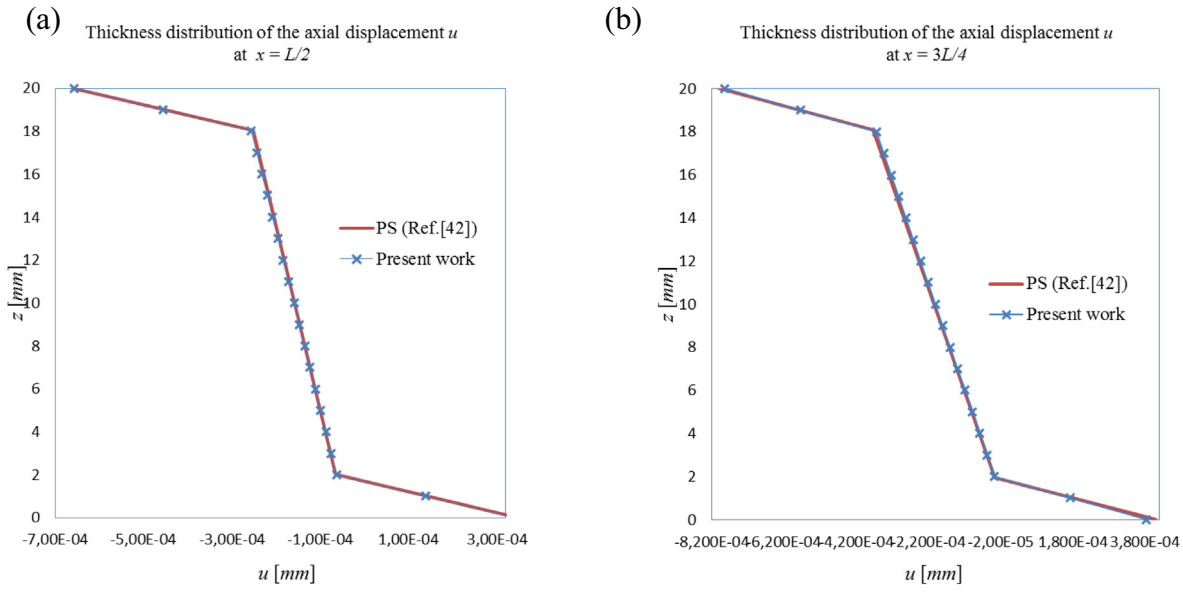

Fig. 10. Non symmetric (composite C) cantilever thick beam ($\lambda = 5$) under end point load. Thickness distribution of the axial displacement (a) at $x = L/2$ and (b) at $x = 3L/4$.

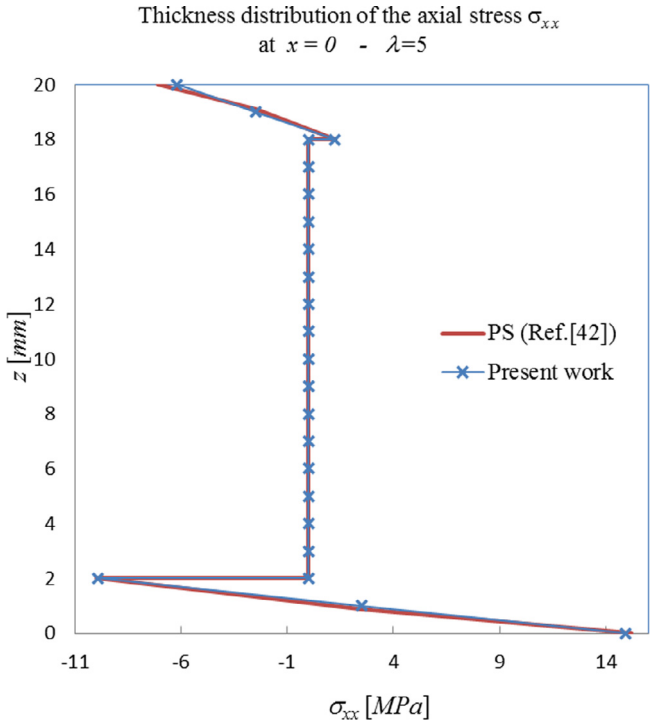

Fig. 11. Non symmetric (composite C) cantilever thick beam ($\lambda = 5$) under end point load. Thickness distribution of the axial stress σ_{xx} at $x = 0$.

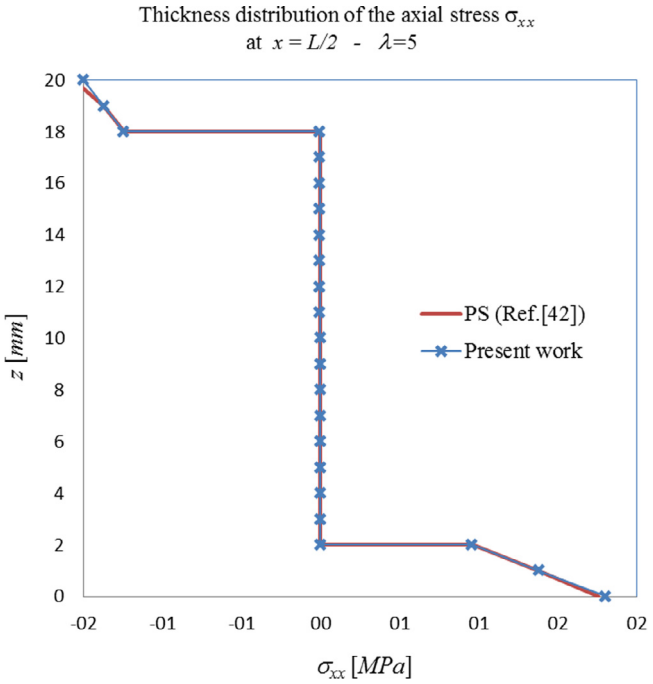

Fig. 12. Non symmetric (composite C) cantilever thick beam ($\lambda = 5$) under end point load. Thickness distribution of the axial stress σ_{xx} at $x = L/2$.

that transverse shear stresses τ_{xz} they are computed from the constitutive equations (Eq. (1)) and from the equilibrium equation (Eq. (45)) and labeled, respectively, as "Present-const" or "Present-equil". At the same time the reference values are labeled as "PS" for results from plane stress and "RI" for results using two-noded linear beam element with reduced integration.

Fig. 14 shows the distribution of the transverse deflection along the beam length obtained with PRZ and are compared with RI reference values, very good agreement is found. Fig. 15 shows the thickness distribution of the normal axial stress at $x = L/4$ and at the mid-section ($x = L/2$). The accuracy of results obtained by the present PRZ approach, employing 8 GS orthogonal polynomials, is noticeable and they are very close to the PS solution. Finally, Fig. 16 shows the distribution of the shear stress τ_{xz} along the thickness for a section located next to the left support ($x = L/20$) and for a section at $x = L/4$. In this last case the average transverse shear stress for each layer (obtained from the constitutive equation) are compared with RI results, showing a very good agreement.

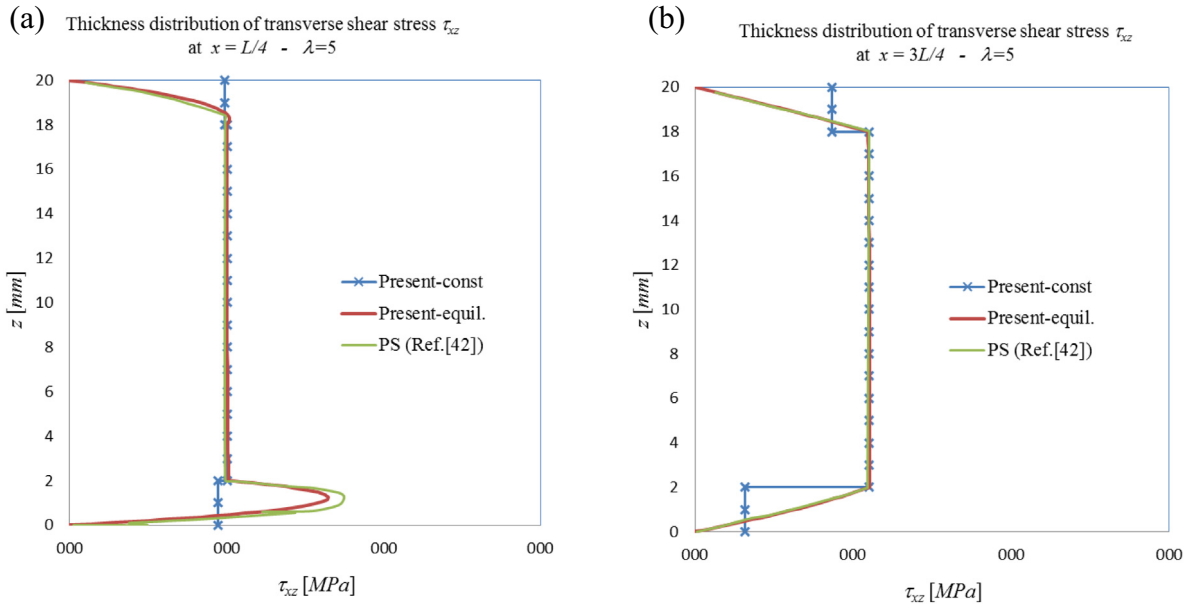

Fig. 13. Non symmetric (composite C) cantilever thick beam ($\lambda = 5$) under end point load. Thickness distribution of transverse shear stress τ_{xz} at a) $x = L/4$ and b) $x = 3L/4$.

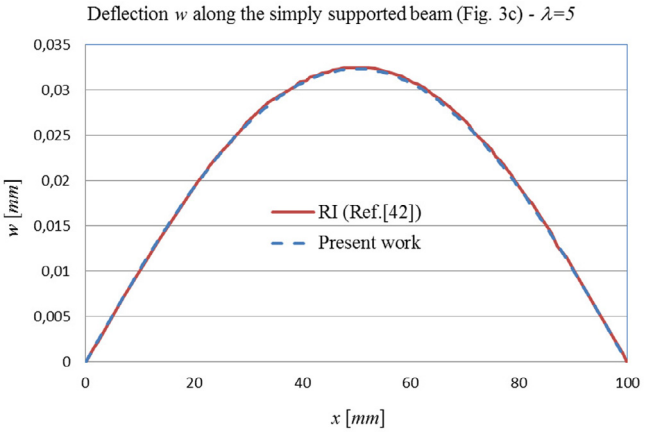

Fig. 14. Simply supported non-symmetric laminated (Composite D) thick beam. Vertical deflection w along the beam length.

8. Modeling of delamination with the PRZ element

The analysis and numerical modeling of damage and failure in laminated beams is complex task. One of the most important failure mechanisms in these kinds of structures is delamination. For instance Di Sciuva and Gherlone [63] used Hermitian zigzag theory and sub-laminate approach and analyzed damage interface increasing the number of variables. Oñate et al. [42] shows that the two-noded element LRZ element developed by them can reproduce the delamination effects in laminated beams without introducing additional kinematic variables. This section proves that the PRZ element has the same property. As is it well known, delamination is produced when the mechanical properties of the interface layer are drastically reduced to almost a zero value in comparison with those of the adjacent layer [64,65]. This delamination model has been applied by Oñate et al. [42] to test the performance of their LRZ into this class of study. Now the mentioned model is applied to show the capacity of this new PRZ hierarchical

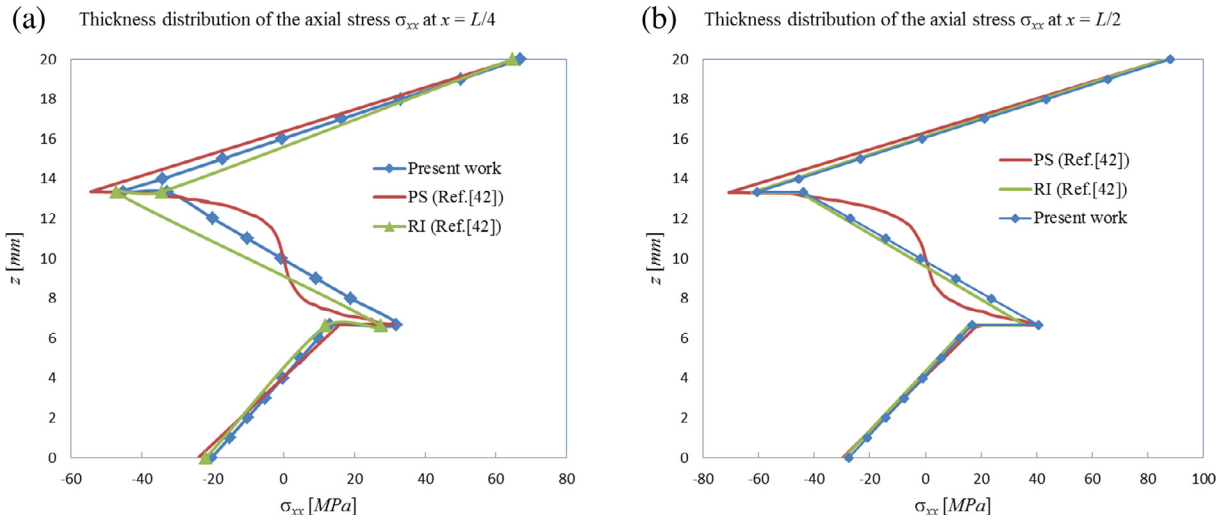

Fig. 15. Simply supported thick beam (Composite D) $\lambda = 5$. Thickness distribution of axial stress σ_{xx} at a) $x = L/4$ and b) $x = L/2$.

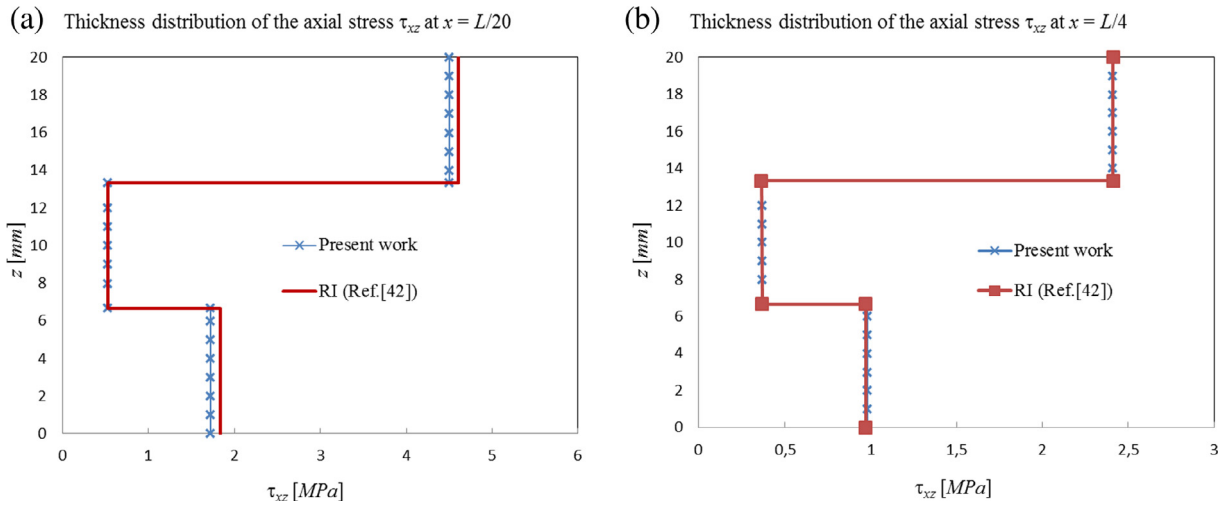

Fig. 16. Simply supported thick beam (Composite D) $\lambda = 5$. Thickness distribution of transverse shear stress τ_{xz} at a) $x = L/20$ and b) $x = L/4$.

element to consider the loss of overall rigidity of the beam due to delamination, leading to an increase in displacement field components.

For this analysis a simply supported beam subjected to a sinusoidal distributed load, as shown in Fig. 3b, is adopted. The reasons for such election are the possibility of comparing with results obtained by programing the Pagano 3D solution [46], which can be certainly determined in this case. The thick laminated beam is made of two layers, with length-to-thickness ratio $\lambda = 5$. The remaining geometrical and mechanical properties are given in Table 8. Delamination between the two layers (bottom and top layers) is taken into account by introducing a very thin interface layer (layer 2 in Table 8) with identical initial properties to the top layer. Next, the transverse shear modulus of the interface layer (G_2) is progressively reduced from Model 1 to Model 12 as shown in Table 9.

Fig. 17 shows the mid span deflection of the laminated beam for Models 1 to 12, i.e. as a function of the shear transverse modulus of the interface, obtained with the present PRZ element and 10 GS enrichment polynomials. In the same figure results obtained applying the 3D Pagano solution have been included. Same interesting features are highlighted; first the mid-span deflection does not significantly change for models 1–5 and them for models 8–11 and second, as a logical conclusion, the main rigidity global beam changes occurs when the shear transverse modulus G_2 varies between 8.76E−001 MPa and 8.76E−004 MPa. Results are in good

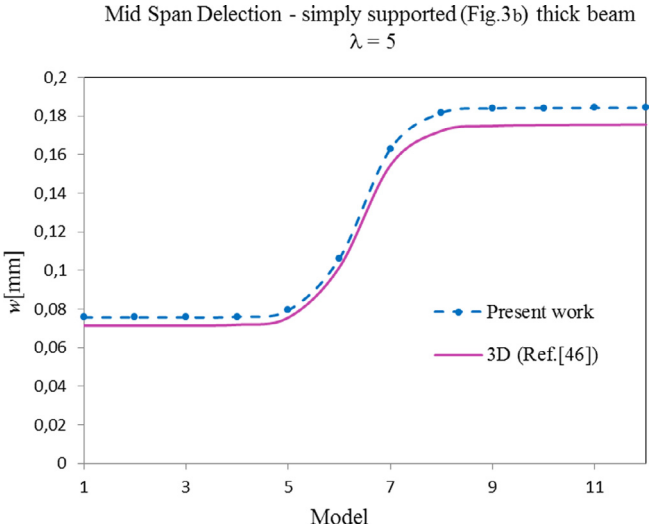

Fig. 17. Delamination study in 2-layered simply-supported thick beam under sinusoidal load. Evolution of mid span transverse deflection with shear modulus G_2 according to Table 9.

agreement with those computed from the 3D Pagano solution. The differences are less than 6%, and it should be noted that the 3D deflection, for comparison purpose, was obtained as the weighted deflection in the thickness beam at $x = L/2$.

Fig. 18 shows the thickness distribution of the axial stresses σ_{xx}, at $x = L/4$, for six decreasing values of shear modulus designed by the corresponding models: 1, 3, 6, 7, 9, 12. The jump of the normal stresses at the interface layer due to delamination is well captured by the PRZ element. Theses stresses at the interface layer remains stationary after a reduction of the material properties of six orders of magnitude. It is important to note the excellent concordance

Table 8
Thickness and layer properties for delamination study in a 2-layered beam. G_2 values are depicted in Table 9.

	Layer 1 (bottom)	Layer 2	Layer 3 (top)
h[mm]	14	0.01	6
E[Mpa]	0.073E+05	2.19E+05	2.19E+05
G[Mpa]	0.029E+05	Model	8.76E+04

Table 9
Shear modulus G_2 in MPa, for the interface layer for delamination analysis.

Model	G_2	Model	G_2	Model	G_2
1	8.76E+004	5	8.76E+000	9	8.76E−004
2	8.76E+003	6	8.76E−001	10	8.76E−005
3	8.76E+002	7	8.76E−002	11	8.76E−006
4	8.76E+001	8	8.76E−003	12	8.76E−007

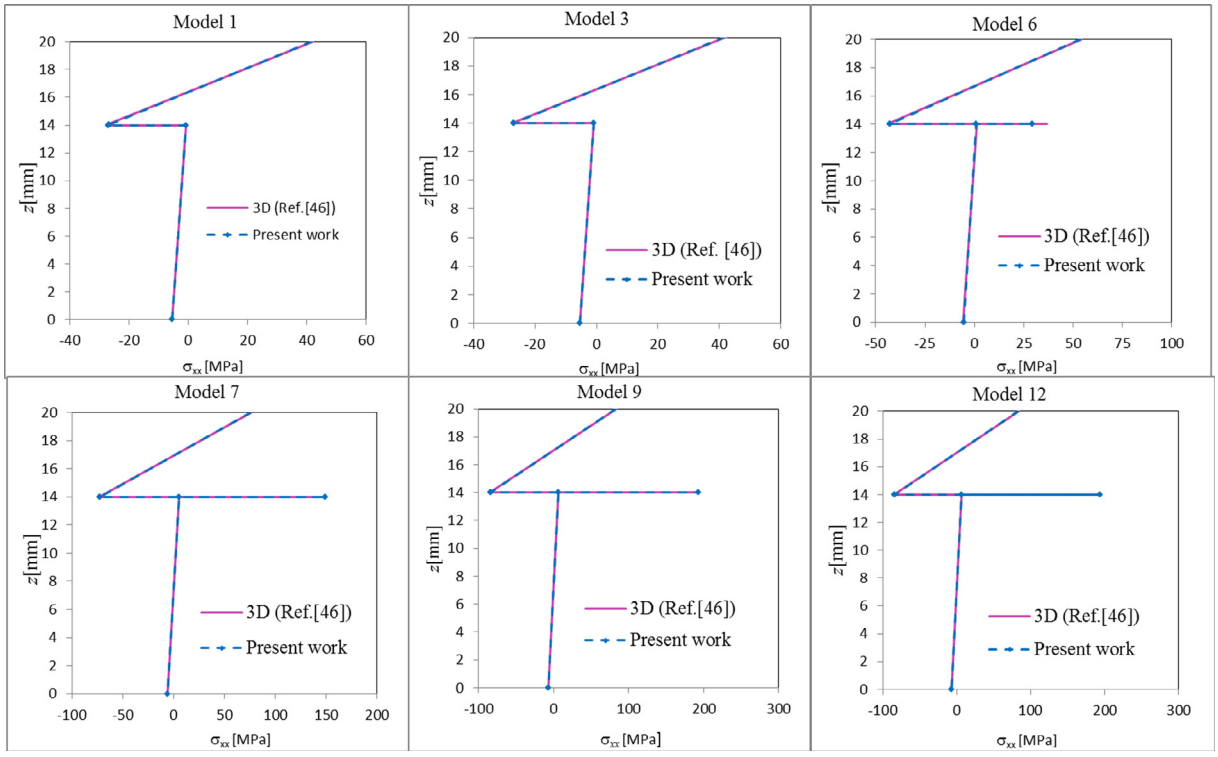

Fig. 18. Delamination study in 2-layered simply-supported thick beam under sinusoidal load. Thickness distribution of normal axial stresses at $x = L/4$ for decreasing shear modulus G_2 form models 1, 3, 6, 7, 9 and 12. (3D obtained after Pagano [46]).

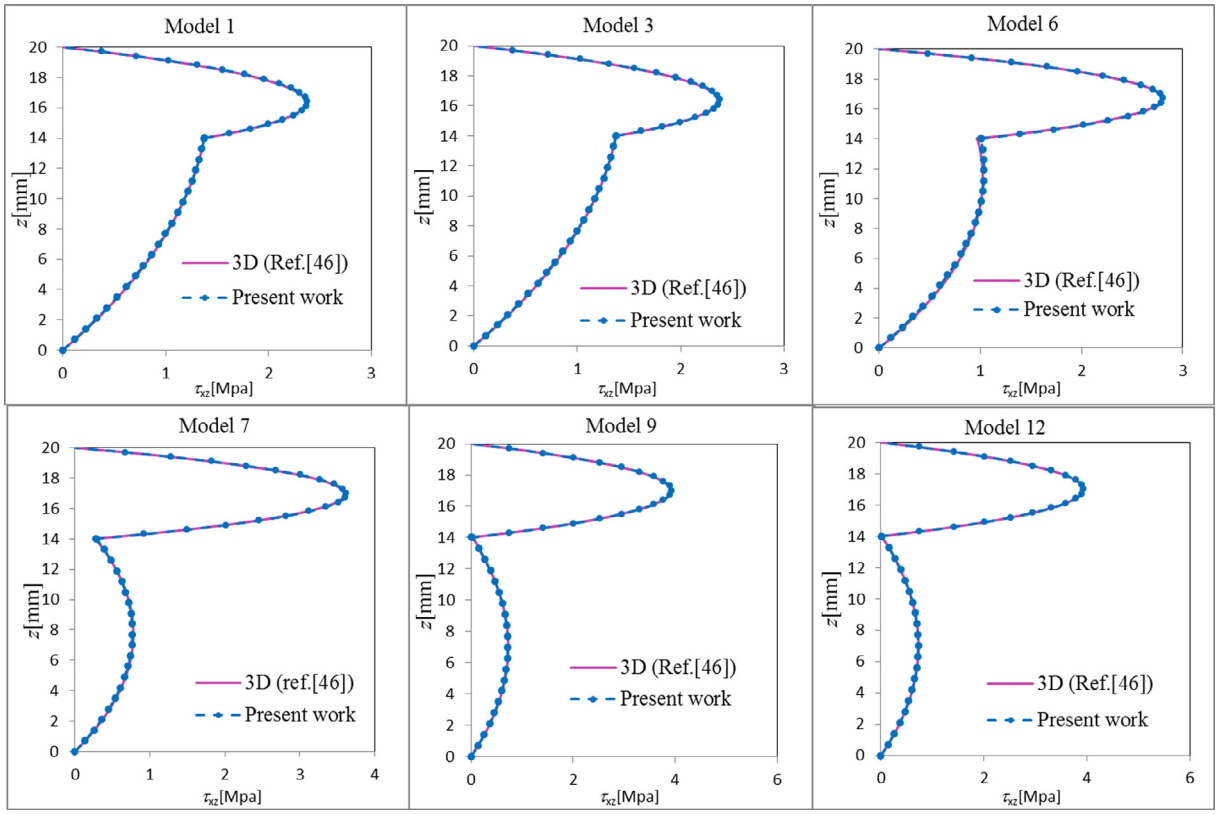

Fig. 19. Delamination study in 2-layered simply-supported thick beam under sinusoidal load. Thickness distribution of normal axial stresses at $x = L/4$ for decreasing shear modulus G_2 form models 1, 3, 6, 7, 9 and 12. (3D obtained after Pagano [46]).

with the 3D solution that has been obtained applying the Pagano solution [46].

Fig. 19 shows the thickness distribution of the transverse shear stresses τ_{xz}, at $x = L/4$, for the same six decreasing values of shear modulus designed by the corresponding models: 1, 3, 6, 7, 9, 12. The shear stresses have been obtained using the present PRZ element by integrating the equilibrium equation. This Figure also includes the corresponding shear stresses obtained by applying Pagano's analytical 3D formulation. Note again the noticeable agreement between the two solutions. Once again the accuracy of PRZ element to capture the delamination effects is demonstrated.

9. Conclusions

A hierarchical beam finite element based on the *p*-version of FEM, using the kinematics of the Tessler's refined zigzag theory, for the analysis of laminated composite beams, has been developed. Recall that the advantages of the *p*-version are not limited to the greater convergence rate. In fact, with *h* methods, the accuracy of the solution is determined by executing several analyses with different meshes, an expensive and time-consuming process, both because of the computational cost and because of the operator time required to define the different models, including de meshing process. In *p*-convergent approximations, the number of finite elements is determined by the geometry and is small. Specifically, all the examples presented in this work require a single hierarchical finite element for the whole beam to obtain the mechanical responses, which are very accurate. Moreover, to verify the results, the order of the approximation (hierarchical modes) can be selectively increased. This operation is carried out very efficiently because it is not necessary to generate a new mesh and because the new linear stiffness matrix contains the preceding one. The convergence study has demonstrated that the element proposed requires a moderate number of degrees of freedom for a very good accuracy. Moreover, it can be applied to study thick and thin beams because no shear locking effects were found. Recall that this element not only improves the convergence and avoids the shear locking, but also requires a few hierarchical Gram-Schmidt polynomials for the same level of accuracy. As a further matter, to verify the results, the order of the approximation can be selectively increased. This operation is carried out very efficiently because it is not necessary to generate a new mesh and because the new linear stiffness matrix contains the preceding ones. The possibility of this new element to consider delamination effects has been clearly demonstrated. On the other side, the hierarchical finite element proposed allows to take into account all coupling effects in an efficient and unified procedure. For this reason, the developed PRZ element can be applied to the analysis of laminated beam with functionally graded materials or damage profile at laminar levels, and it is currently studied by the authors.

Acknowledgments

First author acknowledges financial support from CONICET and MINCyT (Argentina). This work has also been supported by European Research Council through of Advanced Grant: ERC-2012-AdG 320815 COMP-DES-MAT "Advanced tools for computational design of engineering materials", by the Spanish Ministerio de Economia y Competividad through the project: MAT2014-60647-R "Multi-scale and multi-objective optimization of composite laminate structures (OMMC)", and by International Center for Numerical Method in Engineering (CIMNE). All this support is gratefully acknowledged. F. Flores acknowledges financial support from CONICET (Argentina) and SeCyT-UNC.

References

[1] Carrera E. Historical review of zig-zag theories for multilayered plates and shells. Appl Mech Rev 2003;56:65–75.
[2] Carrera E. Theories and finite elements for multilayered, anisotropic, composite plates and shells. Arch Comput Methods Eng 2002;9:87–140.
[3] Carrera E. Theories and finite elements for multilayered plates and shells: a unified compact formulation with numerical assessment and benchmarks. Arch Comput Methods Eng 2003;10:215–96.
[4] Demasi L. ∞6 Mixed plate theories based on the generalized unified formulation. Part I: Governing equations. Compos Struct 2009;87:1–11.
[5] Demasi L. ∞6 Mixed plate theories based on the generalized unified formulation. Part II: layerwise theories. Compos Struct 2009;87:12–22.
[6] Demasi L. ∞6 Mixed plate theories based on the generalized unified formulation. Part III: advanced mixed high order shear deformation theories. Compos Struct 2009;87:183–94.
[7] Demasi L. ∞6 Mixed plate theories based on the generalized unified formulation. Part IV: zig-zag theories. Compos Struct 2009;87:195–205.
[8] Demasi L. ∞6 Mixed plate theories based on the generalized unified formulation. Part V: results. Compos Struct 2009;88:1–16.
[9] Timoshenko S. Theory of elasticity. New York: McGraw-Hill Book Company Inc; 1934.
[10] Pai FP. A new look at shear correction factors and warping functions of anisotropic laminates. Int J Solids Struct 1995;32:2295–313.
[11] Reddy JN. A simple higher – order theory for laminated composite plates. J Appl Mech. Trans ASME 1984;51(4):745–52.
[12] Murty AVK. Toward a consistent beam theory. AIAA J 1984;22(6):811–6.
[13] Surana K, Nguyen S. Two-dimensional curved beam element with higher order hierarchical transverse approximation for laminated composites. Comput Struct 1990;36:499–511.
[14] Matsunaga H. Vibration and buckling of multilayered composite beams according to higher order deformation theories. J Sound Vib 2001;246(1):47–62.
[15] Touratier M. An efficient standard plate theory. Int J Eng Sci 1991;19(8):745–52.
[16] Touratier M. A refined theory of laminated shallow shells. Int J Solids Struct 1992;29(11):1401–15.
[17] Ferreira AJM, Roque CMC, Jorge RMN. Analysis of composite plates by trigonometric shear deformation theory and multiquadrics. Comput Struct 2005;83(27):2225–37.
[18] Vidal P, Polit O. A family of sinus finite elements for the analysis of rectangular laminated beams. Compos Struct 2008;84(1):56–72.
[19] Karama M, Afaq KS, Mistou S. Mechanical behavior of laminated composite beam by the new multi-layered laminated composite structures model with transverse shear stress continuity. Int J Solids Struct 2003;40(6):1525–46.
[20] Aydogdu M. A new shear deformation theory for laminated composite plates. Compos Struct 2009;89(1):94–101.
[21] Mantari JL, Oktem AS, Guedes Soares C. Static and dynamic analysis of laminated composite and sandwich plates and shells by using a new higher-order shear deformation theory. Compos. Struct 2011;94:37–49.
[22] Soldatos KP. A transverse shear deformation theory for homogenous monoclinc plates. Acta Mech. 1992;94:195–220.
[23] Neves AMA, Ferreira AJM, Carrera E, Cinefra M, Roque CMC, Jorge RMN, et al. Free vibration analysis of functionally graded shells by a higher-order shear deformation theory and radial basis functions collocation, accounting for through-the-thickness deformations. Eur J Mech A Solids 2013;37:24–34.
[24] Carrera E, Filippi M, Zappino E. Laminated beam analysis by polinomial, trigonometric, exponential and zig-zag theories. Euro J Mech A/Solids 2013;41:58–9.
[25] Vidal P, Gallimard L, Polit O. Composite beam finite element based on the proper generalized decomposition. Comput Struct 2012;102–103:76–86.
[26] Chakrabarti A, Chalak HD, Iqbal MA, Sheikh AH. A new FE model based on higher order zigzag theory for the analysis of laminated sandwich beam with soft core. Review. Compos Struct 2011;93:271–9.
[27] Robbins DHJ, Reddy JN. Modeling of thick composites using a layer-wise theory. Int J Numer Methods Eng 1993;36:655–77.
[28] Srinivas S. A refined analysis of composite laminates. J Sound Vib 1973;30:495–507.
[29] Reddy JN. Generalization of two-dimensional theories of laminated composite plates. Commun Appl Numer Methods 1987;3:173–80.
[30] Toledano A, Murakami H. A composite plate theory for arbitrary laminate configuration. J Appl Mech 1987;54:181–9.
[31] Lu X, Liu D. An interlaminar shear stress continuity theory for both thin and thick composite laminates. J Appl Mech 1992;59:502–9.
[32] Lee CY, Liu D. An interlaminar stress continuity theory for laminated composite analysis. Comput Struct 1992;42:69–78.
[33] Pai P, Palazotto A. A higher-order sandwich plate theory accounting for a 3-d stresses. Int J Solids Struct 2001;38:5045–62.
[34] Ferreira A. Analysis of composite plates using a layerwise shear deformation theory and multiquadrics discretization. Mech Adv Mater Struct 2005;12:99–112.
[35] Murakami H. Laminated composite plate theory with improved in-plane responses. J Appl Mech 1986;53:661–6.
[36] Lee SP, Senthilnathan NR, Lim SP, Chow ST. An improved zigzag model for the bending of laminated composite plates. Compos Struct 1990;15:137–48.

[37] Cho M, Parmerter RR. Efficient higher order composite plate theory for general lamination configurations. AIAA J 1993;31(7):1299–306.
[38] Cho YB, Averill RC. An improved theory and finite element model for laminated beams using first order zigzag sub-laminate approximations. Compos Struct 1997;37:281–98.
[39] Vidal P, Polit O. Assessment of the refined sinus model for the non-linear analysis of composite beams. Compos Struct 2009;87:370–81.
[40] Vidal P, Polit O. A sine finite element using a zig-zag function for the analysis of laminated composite beams. Compos: Part B 2011;42:1671–82.
[41] Groh RMJ, Weaver PM. On displacement-based and mixed-variational equivalent single layer theories for modelling highly heterogeneous laminated beams. Int J Solids Struct 2015;59:147–70.
[42] Oñate E, Eijo A, Oller S. Simple and accurate two-noded beam element for composite laminated beams using a refined zigzag theory. Comput Methods Appl Mech Eng 2012;213–216:362–82.
[43] Tessler A, Di Sciuva M, Gherlone M. Refinement of Timoshenko beam theory for composite and sandwich beams using zigzag kinematics. Technical Publication 215086. National Aeronautics and Space Administration; 2007
[44] Tessler A, Di Sciuva M, Gherlone M. A refined zig-zag beam theory for composite and sandwich beams. J Compos Mater 2009;43(9):1051–81.
[45] Tessler A, Di Sciuva M, Gherlone M. A consistent refinement of first-order shear deformation theory for laminated composite and sandwich plates using improved zigzag kinematics. J Mech Mater Struct 2010;5(2):341–67.
[46] Pagano N. Exact solutions for rectangular bidirectional composites and sandwich plates. J Compos Mater 1970;4:20–34.
[47] Daví G, Milazzo A, Orlando C. An analytical solution for multilayered beams subjected to ends loads. Compos Struct 2014;116:772–81.
[48] Zienkiewicz OC, Taylor RL. The finite element method. London: McGraw-Hill; 1988.
[49] Szabó B, Düster A, Rank E. The p-version of the finite element method. encyclopedia of computational mechanics. Wiley Online Library; 2004.
[50] Han W, Petyt M. Geometrically nonlinear vibration analysis of thin, rectangular plates using the hierarchical finite element method—I: the fundamental mode of isotropic plates. Comput Struct 1997;63(2):295–308.
[51] Ribeiro P, Petyt M. Multi-modal geometrical non-linear free vibration of fully clamped composite laminated plates. J Sound Vib 1999;225(1):127–52.
[52] Ribeiro P, Petyt M. Nonlinear vibration of composite laminated plates by the hierarchical finite element and continuation methods. Compos Struct 1999;46(3):197–208.
[53] Szabó BA, Mehta AK. P-convergent finite element approximations in fracture mechanics. Int J Numer Meth Eng 1978;12(3):551–60.
[54] Szabó BA, Babuska I. Finite element analysis. New York: Wiley; 1991.
[55] Ribeiro P. First-order shear deformation, p-version, finite element for laminated plate nonlinear vibrations. AIAA J 2005;43(6):1371–9.
[56] Jones RM. Mechanics of composite materials. 2nd ed. CRC Press; 2015.
[57] Düster A, Rank E. A p-version finite element approach for two- and three-dimensional problems of the J2 flow theory with non-linear isotropic hardening. Int J Numer Methods Eng 2002;53(1):49–63.
[58] Nallim LG, Oller S, Grossi RO. Statical and dynamical behaviour of thin fibre reinforced composite laminates with different shapes. Comput Methods Appl Mech Eng 2005;194:1797–822.
[59] Nallim LG, Oller S. An analytical - numerical approach to simulate the dynamic behaviour of arbitrarily laminated composite plate. Compos Struct J 2008;85:311–25.
[60] Rango RF, Nallim LG, Oller S. Static and dynamic analysis of thick laminated plates using enriched macroelements. Compos Struct J 2013;101:94–103.
[61] Rango RF, Nallim LG, Oller S. Formulation of enriched macro elements using trigonometric shear deformation theory for free vibration analysis of symmetric laminated composite plate assemblies. Compos Struct J 2015;119:38–49.
[62] Rango RF, Nallim LG, Oller S. An enriched macro finite element for the static analysis of thick general quadrilateral laminated composite plates. Mech Adv Mater Struct 2016;23(10):1197–206.
[63] Di Sciuva M, Gherlone M. A global/local third-order Hermitian displacement field with damaged interfaces and transverse extensibility: analytical formulation. Compos Struct 2003;59(4):419–31.
[64] Oller S. Numerical simulation of mechanical behavior of composite materials. Barcelona: Springer; 2015.
[65] Di Capua D, Oñate E. Two-noded zigzag beam element accounting for shear effects based on an extended Euler Bernoulli theory. Compos Struct 2015;132(15):1192–205.